Article

Targeting myeloid chemotaxis to reverse prostate cancer therapy resistance

https://doi.org/10.1038/s41586-023-06696-z

Received: 23 May 2023

Accepted: 28 September 2023

Published online: 16 October 2023

Open access

Check for updates

Christina Guo[1,2,13], Adam Sharp[1,2,13], Bora Gurel[1], Mateus Crespo[1], Ines Figueiredo[1], Suneil Jain[3,4], Ursula Vogl[5], Jan Rekowski[1], Mahtab Rouhifard[1], Lewis Gallagher[1], Wei Yuan[1], Suzanne Carreira[1], Khobe Chandran[1,2], Alec Paschalis[1,2], Ilaria Colombo[5], Anastasios Stathis[5,6], Claudia Bertan[1], George Seed[1], Jane Goodall[1], Florence Raynaud[1], Ruth Ruddle[1], Karen E. Swales[1], Jason Malia[1], Denisa Bogdan[1], Crescens Tiu[1,2], Reece Caldwell[2], Caterina Aversa[2], Ana Ferreira[1], Antje Neeb[1], Nina Tunariu[2], Daniel Westaby[1,2], Juliet Carmichael[1,2], Maria Dolores Fenor de la Maza[1,2], Christina Yap[1], Ruth Matthews[1], Hannah Badham[1], Toby Prout[1], Alison Turner[1], Mona Parmar[1], Holly Tovey[1], Ruth Riisnaes[1], Penny Flohr[1], Jesus Gil[7,8], David Waugh[4,9], Shaun Decordova[1], Anna Schlag[1], Bianca Cali[10], Andrea Alimonti[5,6,10,11,12] & Johann S. de Bono[1,2] ✉

Inflammation is a hallmark of cancer[1]. In patients with cancer, peripheral blood myeloid expansion, indicated by a high neutrophil-to-lymphocyte ratio, associates with shorter survival and treatment resistance across malignancies and therapeutic modalities[2–5]. Whether myeloid inflammation drives progression of prostate cancer in humans remain unclear. Here we show that inhibition of myeloid chemotaxis can reduce tumour-elicited myeloid inflammation and reverse therapy resistance in a subset of patients with metastatic castration-resistant prostate cancer (CRPC). We show that a higher blood neutrophil-to-lymphocyte ratio reflects tumour myeloid infiltration and tumour expression of senescence-associated mRNA species, including those that encode myeloid-chemoattracting CXCR2 ligands. To determine whether myeloid cells fuel resistance to androgen receptor signalling inhibitors, and whether inhibiting CXCR2 to block myeloid chemotaxis reverses this, we conducted an investigator-initiated, proof-of-concept clinical trial of a CXCR2 inhibitor (AZD5069) plus enzalutamide in patients with metastatic CRPC that is resistant to androgen receptor signalling inhibitors. This combination was well tolerated without dose-limiting toxicity and it decreased circulating neutrophil levels, reduced intratumour $CD11b^{+}HLA\text{-}DR^{lo}CD15^{+}CD14^{-}$ myeloid cell infiltration and imparted durable clinical benefit with biochemical and radiological responses in a subset of patients with metastatic CRPC. This study provides clinical evidence that senescence-associated myeloid inflammation can fuel metastatic CRPC progression and resistance to androgen receptor blockade. Targeting myeloid chemotaxis merits broader evaluation in other cancers.

Inflammation is a hallmark of cancer[1]. Although T cell-mediated antitumour immunity has been harnessed for the management of some malignancies, myeloid inflammation, reflected by a high neutrophil-to-lymphocyte ratio (NLR) and neutrophilia, is associated with worse overall survival and therapeutic resistance across many malignancies[2–5].

Metastatic prostate cancer is a common cause of male cancer mortality[6]. Existing treatments mainly target tumour cells directly. Treatments aimed at eliciting T cell-mediated immunity have, to date, shown insufficient clinical efficacy, possibly due to relatively low T cell infiltration in CRPC and the presence of immunosuppressive cues[7–9]. Prostate cancer is frequently infiltrated by myeloid inflammatory cells, including $CD11b^{+}HLA\text{-}DR^{lo}CD15^{+}CD14^{-}$ cells (also termed polymorphonuclear myeloid-derived suppressor cells (PMN-MDSCs) or tumour-associated neutrophils) as well as heterogeneous, alternatively differentiated myeloid cells[10–15]. Several groups have shown, using prostate cancer mouse models, that intratumour myeloid cells can drive paracrine oncogenic signalling, senescence evasion and

[1]The Institute of Cancer Research, London, UK. [2]The Royal Marsden NHS Foundation Trust, London, UK. [3]Northern Ireland Cancer Centre, Belfast, UK. [4]Patrick G Johnston Centre for Cancer Research, Queen's University Belfast, Belfast, UK. [5]Oncology Institute of Southern Switzerland, Ente Ospedaliero Cantonale (EOC), Bellinzona, Switzerland. [6]Faculty of Biomedical Sciences, Università della Svizzera Italiana (USI), Lugano, Switzerland. [7]MRC London Institute of Medical Sciences (LMS), London, UK. [8]Institute of Clinical Sciences (ICS), Faculty of Medicine, Imperial College London, London, UK. [9]Centre for Cancer Biology, University of South Australia, Adelaide, South Australia, Australia. [10]Institute of Oncology Research, Bellinzona, Switzerland. [11]Department of Health Sciences and Technology, Eidgenössische Technische Hochschule Zürich (ETH), Zurich, Switzerland. [12]Department of Medicine, Veneto Institute of Molecular Medicine, University of Padova, Padua, Italy. [13]These authors contributed equally: Christina Guo, Adam Sharp. ✉e-mail: johann.debono@icr.ac.uk

immunosuppression[10–12,14–17]. This is supported by observations of increases in intratumour CD11b$^+$HLA-DR^{lo}CD15$^+$CD14$^-$ cells with progression from treatment-naive to metastatic CRPC (mCRPC)[10]. Moreover, overexpression of a myeloid-specific signature on whole-blood mRNA profiling and high NLR predict shorter overall survival in patients with mCRPC[2,3,18,19]. High NLR also associates with resistance to androgen receptor signalling inhibitors (ARSIs)[3].

Preclinical studies indicate that recruitment of myeloid cells into prostate tumours is at least in part driven by tumour-derived chemokines binding to CXCR2 (refs. 10,12,14,15). CXCR2 ligands have been shown to be upregulated in response to tumour-suppressor loss and oncogenic activation[12,15,20–22]. Some of the mainstays of prostate cancer treatment—radiotherapy and androgen deprivation therapy—can also trigger upregulation of CXCR2 ligands, which constitute a part of the senescence-associated secretory phenotype (SASP)[10,12,14,23]. In models of different tumours, including prostate cancer, CXCR2 inhibition blocks the recruitment of tumour-infiltrating PMN-MDSCs leading to tumour suppression[10,12,14,24,25]. However, the extent to which this axis drives myeloid recruitment into the periphery and then into the tumour, and whether these cells contribute to human CRPC progression, are not clear. Critically, whether CXCR2 inhibition can overcome therapeutic resistance and confer clinical benefit to patients with mCRPC has not been evaluated. We reasoned that CXCR2 chemokines released by human prostate cancer cells sculpt systemic myeloid inflammation, and that targeting CXCR2 would decrease deleterious myeloid inflammation, reverse ARSI resistance and impart clinical benefit in some patients with mCRPC.

NLR reflects tumour myeloid infiltration

As circulating and intratumour myeloid inflammation associate with worse prostate cancer outcomes[3,10], we first evaluated associations between the circulating and tumour myeloid compartments. We analysed mCRPC biopsies from 48 patients (cohort 1) treated at 3 hospitals (Royal Marsden (RMH), Oncology Institute of Southern Switzerland and Belfast City Hospital). Most of these patients had previously received at least one ARSI (97.9%) and at least one taxane (95.8%; Supplementary Table 1). The density of myeloid inflammatory cells was quantified by six-colour immunofluorescence (IF) for CD11b, CD15, CD14, HLA-DR, DAPI (nuclear stain) and CXCR2 (Extended Data Fig. 1a). Intratumour CD11b$^+$HLA-DR^{lo}CD15$^+$CD14$^-$ myeloid cell density positively associated with contemporaneously collected peripheral blood NLR and neutrophil counts (Fig. 1a–c). There was no significant association between CD11b$^+$HLA-DR^{lo}CD15$^-$CD14$^+$ (also termed monocytic) myeloid cell density and peripheral blood NLR or neutrophil count (Extended Data Fig. 1b,c). We validated this positive association between CD11b$^+$HLA-DR^{lo}CD15$^+$CD14$^-$ myeloid cell density and peripheral blood NLR, as well as neutrophil count, in a further cohort of 57 patients with mCRPC treated at the RMH (validation cohort), where most patients had received at least one ARSI (91.2%) and at least one taxane (93.0%; Extended Data Fig. 1d,e and Supplementary Table 1). The positive associations between NLR, and circulating neutrophil counts, and tumour biopsy myeloid cell infiltration were statistically significant irrespective of the biopsy sites in both cohorts (Supplementary Table 2).

CXCR2 ligands and myeloid inflammation

Given the association between peripheral and intratumour myeloid compartments, we reasoned that intratumour CD11b$^+$HLA-DR^{lo}CD15$^+$CD14$^-$ cell infiltration is driven by tumour-derived chemokines. First, we carried out transcriptome analyses associating peripheral blood NLR and neutrophil count with the expression of pan-immune genes (770 gene list from the nCounter PanCancer Immune Profiling Panel[26]) in bulk RNA-sequencing (RNA-seq) data from contemporaneously collected mCRPC biopsies from 95 patients treated at the RMH[27] who had received at least one taxane and one ARSI. These mCRPC biopsy RNA-seq analyses showed that eight senescence- and myeloid-associated transcripts, including *CXCL1*, *CXCL2*, *CXCL8* (*IL8*), *IL1RN* (*IL1RA*), *CD68*, *PLAUR*, *NFKB1* and *CEBPB*, were among the top 20 genes most positively associated with NLR. CXCL1, CXCL2 and CXCL8 are ligands for CXCR2, implicated in the SASP and myeloid chemotaxis[21,28,29]. C/EBPβ and NF-κB have been shown to modulate the transcription of the CXCR2 ligands CXCL1, CXCL2 and CXCL8 (Fig. 1d and Extended Data Fig. 1f; refs. 21,30–32). Next, we determined whether the genes encoding these ligands associate with intratumour myeloid inflammation. The expression of *CXCL1*, *CXCL2*, *IL1RN* and *PLAUR* positively associated with two previously published myeloid gene signatures[10,33] in the Stand Up To Cancer–Prostate Cancer Foundation (SU2C–PCF)[34] and RMH CRPC RNA-seq datasets[27]. The associations between *CEBPB* (RMH) and *CXCL8* (SU2C–PCF) with both myeloid gene signatures were observed in one of the two datasets (Supplementary Table 3).

To elucidate the clinical relevance of the CXCR2 axis in mCRPC, we carried out survival analyses for the CXCR2 ligands using these two RNA-seq datasets. Higher expression levels of *CXCL1*, *CXCL2*, *CXCL3*, *CXCL5*, *CXCL6* and *CXCL8* were negatively prognostic for overall survival from the time of CRPC biopsy in the SU2C–PCF cohorts. *CXCL1*, *CXCL2*, *CXCL3* and *CXCL7* were also negatively prognostic in the RMH cohort (Fig. 1e–g and Extended Data Fig. 2a–k). Overall, these data indicate that in patients with mCRPC, high peripheral blood NLR and neutrophilia associate with tumour cell expression of senescence-related transcripts, including those for CXCR2 chemokine ligands that can chemoattract myeloid cells into tumour, with the expression of these chemokines being negatively prognostic.

Myeloid cells in CRPC express CXCR2

We next investigated CXCR2 expression on tumour and immune cells in human prostate cancer. We interrogated two publicly available single-cell RNA-seq datasets of CRPC samples from 14 patients[35] and localized prostate cancer samples from 11 patients[36]. CXCR2 was specifically expressed and at high levels by cells clustered as neutrophils, with minimal tumour cell expression (Fig. 1h and Extended Data Fig. 2l). We next evaluated mCRPC biopsies from 14 patients with CRPC (a subset of cohort 1) who had received at least one ARSI to determine CXCR2 protein expression on tumour cells and immune cells of the following phenotypes: CD11b$^+$HLA-DR^{lo}CD15$^+$CD14$^-$ myeloid cells, CD11b$^+$HLA-DR^{lo}CD15$^-$CD14$^+$ myeloid cells, lineage-marker-negative (Lin$^-$) CD11b$^+$HLA-DR^{lo}CD15$^-$CD14$^-$ myeloid cells, CD68$^+$CD206$^-$CD163$^-$ macrophages, CD68$^+$ macrophages expressing CD206 and/or CD163, CD4$^+$FOXP3$^+$ regulatory T cells, CD4$^+$FOXP3$^-$ T helper cells, T cells positive for CD8 and granzyme B (GzB), CD8$^+$GzB$^-$ T cells, CD20$^+$CD138$^-$MUM1$^-$ B cells, CD20$^+$ B cells expressing MUM1 and/or CD138, pan-CK$^+$ cells without biomarkers associated with a neuroendocrine phenotype (synaptophysin (Syn), CD56 and chromogranin (CgA)) and pan-CK$^+$ tumour cells expressing at least one of the biomarkers associated with a neuroendocrine phenotype (Supplementary Figs. 1 and 2).

Consistent with the single-cell RNA-seq results, the data on the expression of membranous CXCR2 protein showed that it was expressed by most CD11b$^+$HLA-DR^{lo}CD15$^+$CD14$^-$ myeloid cells, and to a lesser extent by other myeloid subsets, but was largely undetectable on non-myeloid cells (Fig. 1i). Interrogation of cohort 1 (n = 48 patients) and the validation cohort (n = 57 patients) also showed that CXCR2 was expressed by most CD11b$^+$HLA-DR^{lo}CD15$^+$CD14$^-$ cells in CRPC biopsies, and the frequency of expression did not differ significantly across metastatic sites (Extended Data Fig. 2m,n). The selective and frequent expression of CXCR2 by CD11b$^+$HLA-DR^{lo}CD15$^+$CD14$^-$ myeloid cells in CRPC biopsies makes it an attractive therapeutic target.

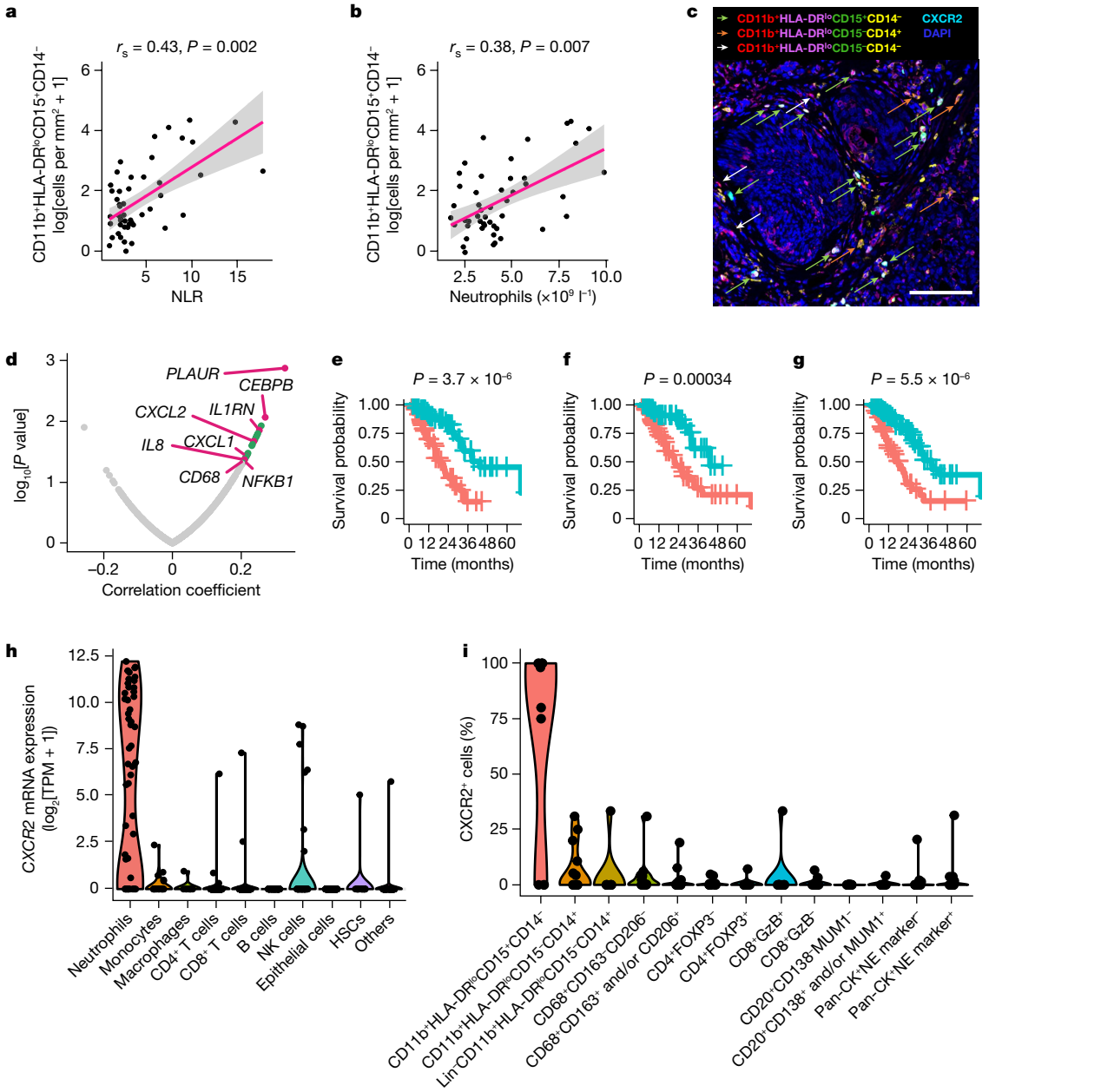

Fig. 1 | Prostate tumour cells generate CXCR2 chemokines associated with tumour and peripheral myeloid inflammation. a,**b**, Scatter plots of log-transformed intratumour CD11b$^+$HLA-DR^{lo}CD15$^+$CD14$^-$ cell density versus NLR (**a**) and neutrophil count (**b**) in patients with mCRPC (cohort 1, $n = 48$). Shown are estimated linear regression lines (pink) with 95% confidence intervals (grey), correlation coefficients, and *P* values from the two-sided Spearman's rank correlation analyses. **c**, Micrograph showing a six-colour IF panel example of a human mCRPC biopsy stained for CD11b, HLA-DR, CD15, CD14 and CXCR2 and with DAPI, with arrows depicting different myeloid subsets. Scale bar, 100 µm. Entire slides were scanned and analysable slide areas were quantified for **a**,**b**. **d**, Volcano plot of the top 20 immune transcripts (green and pink) expressed in mCRPC biopsy bulk transcriptomes (RMH cohort, $n = 95$) that most positively associated with NLR. Pink, SASP genes and CXCR2 chemokines. **e**–**g**, Kaplan–Meier plots of overall survival from the time of CRPC biopsy based on gene expression of CXCL1 (**e**), CXCL2 (**f**) and CXCL8 (**g**) in CRPC bulk transcriptomes from the SU2C–PCF ($n = 141$) cohort. Gene expression cutoff was determined using the optimized Maxstat method. Blue line, low expression; red line, high expression. *P* values were calculated using the log-rank test. **h**, Violin plot of *CXCR2* mRNA expression from single-cell RNA-seq data from 15 advanced prostate cancer biopsies (14 patients). TPM, transcripts per million; NK, natural killer; HSCs, haematopoietic stem cells. **i**, Violin plots by proportion of intratumour immune cell and tumour cells staining for CXCR2 protein in human mCRPC biopsies ($n = 14$). NE, neuroendocrine.

Clinical trial of CXCR2 inhibitor plus ARSI

We next administered a CXCR2 inhibitor (CXCR2i) to patients with mCRPC progressing after at least one ARSI in an investigator-initiated clinical trial, to generate proof-of-mechanism data showing that CXCR2i can reduce peripheral and tumour myeloid infiltration, as well as to pursue proof-of-concept evidence that inhibition of myeloid infiltration can reverse clinical ARSI resistance. This was a dose-finding, phase 1 trial of a selective CXCR2i, AZD5069 (40 mg twice daily (BD) to 320 mg BD), combined with enzalutamide (160 mg once daily (OD)) in patients with ARSI-resistant mCRPC using a 3 + 3 design. The primary trial objective was to evaluate the safety and tolerability of the combination. Key secondary objectives were to evaluate pharmacokinetic–pharmacodynamic parameters and antitumour activity. Administration

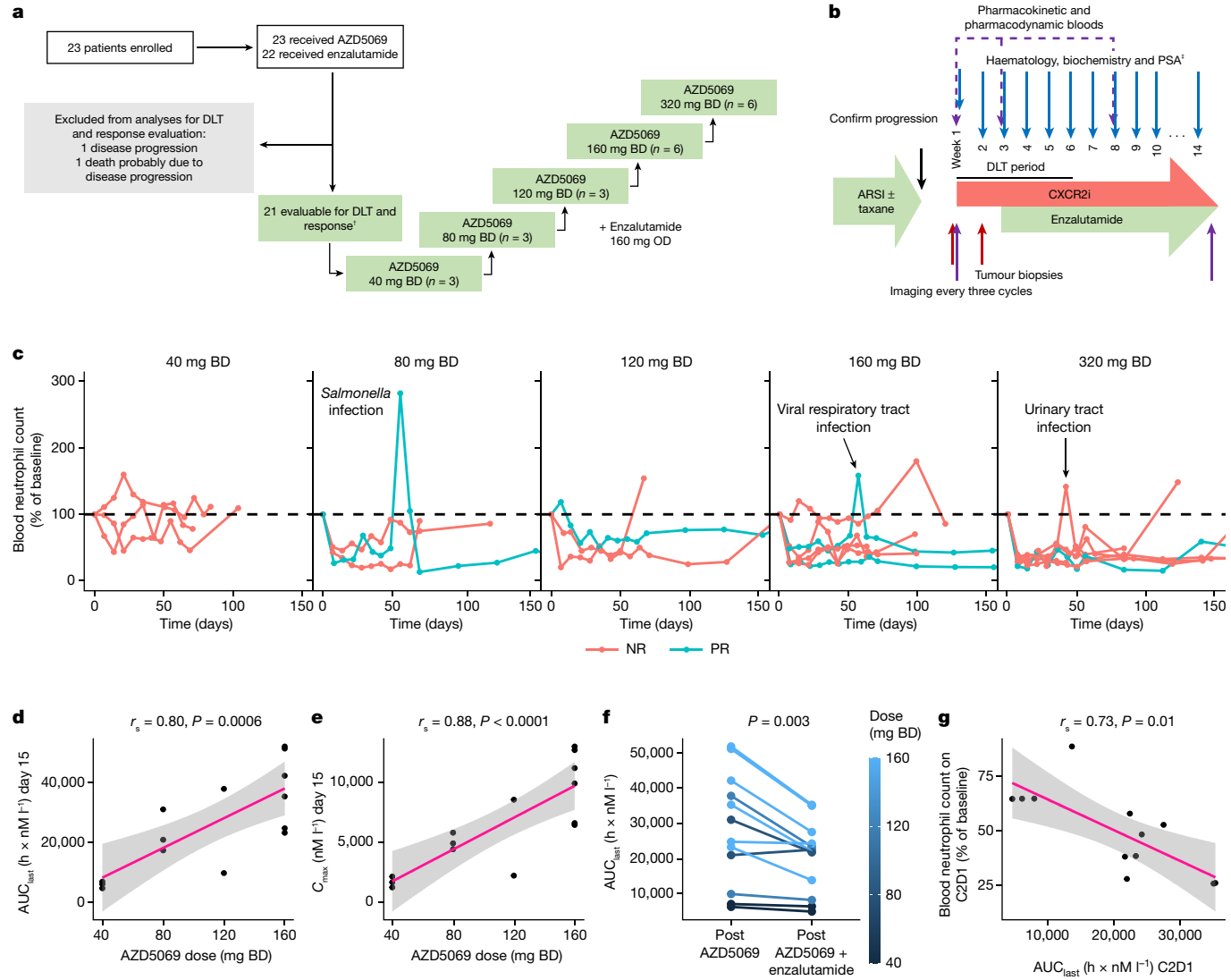

Fig. 2 | CXCR2 blockade leads to dose-dependent, on-target neutropaenia. **a**, Patient disposition per Consolidated Standards of Reporting Trials guidelines. †Two patients were replaced per protocol after coming off study before completing the DLT period for a reason other than a DLT, and therefore were not evaluable for the primary endpoint or response. **b**, Clinical trial schema. Patients had confirmed disease progression on androgen deprivation therapy and at least one ARSI. Week count relative to the commencement of AZD5069 administration is shown. Cohorts 1–4 started AZD5069 2 weeks before enzalutamide; cohort 5 started drugs concurrently. ‡PSA test was carried out on day 1 of each cycle. **c**, By-patient, serial, peripheral blood neutrophil counts for each dose level of AZD5069. All available data points up to day 150 are shown. NR, patient classed as a non-responder; PR, patient classed as a partial responder. **d**, Scatterplot of AZD5069 dose versus AUC_{last} ($h \times nM\ l^{-1}$) for AZD5069 monotherapy on day 15 of AZD5069 administration at 40 to 160 mg BD ($n = 14$). **e**, Scatterplot of AZD5069 dose and peak concentration (C_{max} ($nM\ l^{-1}$)) on day 15 of AZD5059 administration in patients treated with AZD5069 at 40 to 160 mg BD ($n = 14$). **f**, AZD5069 plasma concentration (AUC_{last} ($h \times nM\ l^{-1}$)) at steady state for AZD5069 monotherapy (after 14 days of monotherapy) versus combination therapy (after 28 days of combined administration of AZD5069 and enzalutamide; $n = 12$ pairs). Two-sided paired Wilcoxon signed-rank test P value is shown. Line colour indicates AZD5069 dose. **g**, Scatterplot of AZD5069 plasma concentration on cycle 2 day 1 (C2D1) (x axis) and blood neutrophil count on C2D1 as a percentage of the value at baseline. For **d**,**e**,**g**, estimated linear regression lines (pink) with 95% confidence interval (grey band), and correlation coefficients and P values from the two-sided Spearman's rank correlation analyses are shown.

of AZD5069 was commenced 2 weeks before that of enzalutamide in all but the 320 mg BD cohort to identify potential pharmacokinetic interactions (Fig. 2a,b). Between November 2017 and November 2022, we enrolled 23 patients with metastatic castration-resistant prostate adenocarcinoma (Extended Data Table 1). All patients were evaluable for safety, having received at least one dose of either study drug. Twenty-one patients were evaluable for dose-limiting toxicities (DLTs). Two patients were not evaluable for the primary endpoint and were replaced per protocol after coming off study for clinical progression and not toxicity after 1 and 6 days on trial before completing the DLT period.

We did not observe any DLT. The most common treatment-emergent adverse events were uncomplicated, dose-dependent, on-target neutropaenia (83%, grade ≥ 3: 48%), fatigue (30%, no grade ≥ 3), nausea (22%, no grade ≥ 3), anaemia (17%, grade ≥ 3: 4%), leukopaenia (13%, no grade ≥ 3), headache (13%, no grade ≥ 3), constipation (9%, no grade ≥ 3) and thrombocytopaenia (9%, no grade ≥ 3; Extended Data Table 2). Three patients had infections, deemed unrelated to the investigational agents by the safety review committee, and mounted appropriate, transient, neutrophilic responses, supporting the reversible mechanism of AZD5069 in inhibiting myeloid chemotaxis, rather than impairing marrow function or causing leukocyte destruction. Infections

(viral respiratory tract infection and *Salmonella* gastroenteritis) were self-limiting in two patients; urinary tract infection in the third patient with urinary tract outflow obstruction resolved after oral antibiotics (Fig. 2c). There was no permanent treatment discontinuation due to treatment-emergent adverse events. One patient (80 mg BD dose) underwent permanent dose reduction of AZD5069 for grade 4 neutropaenia. One patient died after 6 days on study probably owing to rapidly progressing disease, but no postmortem was carried out so relatedness to the investigational agents could not be unequivocally excluded.

CXCR2i reduced myeloid cell counts

AZD5069 exposure represented by the area under the concentration-time curve from time zero to time of the last quantifiable concentration (AUC_{last}) and maximum concentration (C_{max}) at steady state increased in a dose-dependent manner (Fig. 2d,e), but AZD5069 exposure (AUC_{last}) decreased after the addition of enzalutamide, particularly at the higher dose levels, probably owing to enzalutamide increasing hepatic clearance of AZ5069 by CYP3A4 induction (Fig. 2f). Nonetheless, AZD5069 decreased blood neutrophil counts and NLRs in a dose-dependent manner (Fig. 2c and Extended Data Fig. 3). The association between the degree of neutropaenia and AZD5069 exposure on cycle 2 day 1 also confirms this pharmacokinetic-pharmacodynamic relationship (Fig. 2g). To elucidate the impact of CXCR2i on intratumour myeloid cell infiltration and tumour immune landscape, we carried out hyperplex IF for immune and tumour cell markers on paired tumour biopsies obtained from the same disease site within 1 week prior to and approximately 2 weeks after starting treatment. Biopsies were taken from 18 patients (17 pairs). Thirteen pairs of biopsies were analysable by hyperplex IF as four pairs of samples did not contain sufficient tumour, were too blood stained, or were crushed (Supplementary Table 4).

CXCR2i reduced the density of $CD11b^{+}HLA\text{-}DR^{lo}CD15^{+}CD14^{-}$ myeloid cells in CRPC biopsies of most patients treated with AZD5069 >40 mg BD, doses sufficient to achieve on-target reduction in blood neutrophil counts of at least 30% (Fig. 3a–c). As low HLA-DR is not always used when phenotyping granulocytic myeloid cells, we also examined the impact of CXCR2i on $CD11b^{+}CD15^{+}CD14^{-}$ myeloid cells and observed a consistent change. Notably, the change in $CD11b^{+}HLA\text{-}DR^{lo}CD15^{+}CD14^{-}$ myeloid cell density reflected AZD5069 exposure and blood neutropaenia (Fig. 3d). CXCR2i did not significantly alter the density of other immune cells, which rarely express CXCR2 (Extended Data Fig. 4).

To determine whether CXCR2i led to compensatory ligand upregulation, we serially measured the levels of circulating CXCL1, CXCL2, CXCL5, CXCL6, CXCL7 and CXCL8. CXCL3 was not measured. Notably, the levels of CXCL1, CXCL2 and CXCL8, the only CXCR2 ligands whose gene expression correlated with NLR in our initial analysis (Fig. 1d), increased in a dose-dependent manner after treatment. The degree of neutropaenia on cycle 2 day 1 correlated with the degree of CXCL1, CXCL2 and CXCL8 upregulation at the same time point (Fig. 3e–g and Extended Data Fig. 5). CXCL5, CXCL6 and CXCL7 levels did not consistently increase after CXCR2i or associate with neutropaenia (Extended Data Fig. 5). These findings indicate that CXCR2i can affect granulocytic myeloid cell infiltration; however, compensatory upregulation of ligands that can bind to CXCR1 and/or CXCR2 is a potential resistance mechanism.

CXCR2i can reverse CRPC ARSI resistance

Five (24%) of 21 patients had an objective partial response using the prespecified response criteria of: ≥30% decrease in measurable disease according to the Response Evaluation Criteria in Solid Tumors v.1.1, prostate-specific antigen (PSA) decline ≥50% confirmed ≥4 weeks later, and/or conversion of circulating tumour cell (CTC) count from ≥5 per 7.5 ml of blood at baseline to <5 per 7.5 ml of blood at nadir (Fig. 4a–c). Patients needed to be on treatment for at least 12 weeks to be considered a responder. Thirteen patients had assessable measurable disease by Response Evaluation Criteria in Solid Tumors v.1.1. Eight patients had a baseline CTC count of ≥5 per 7.5 ml of blood. All patients classed as partial responders had radiologic progression-free survival of more than 6 months. Four patients classed as partial responders had confirmed disease progression by Prostate Cancer Working Group 2 criteria on enzalutamide, and one had progressed on abiraterone alone, prior to treatment with AZD5069. Three of four patients classed as partial responders, for whom pre-treatment tissue biopsy was available for androgen receptor splice variant 7 (AR-V7) immunohistochemistry (IHC) including the patient who received only abiraterone previously, had tumour expressing AR-V7 protein. AR-V7 is a reported biomarker of enzalutamide resistance[37].

The patient classed as a partial responder treated with AZD5069 at 320 mg BD had Gleason 9 mCRPC (AR-V7 IHC not available) with progressing high-volume bone metastases on enzalutamide before trial entry (Extended Data Fig. 6). PSA doubling time was 1 month. We observed a 64% PSA reduction (129 ng ml^{-1} to 47 ng ml^{-1}) after four cycles. Whole-body magnetic resonance imaging showed an increase in apparent diffusion coefficient in the bone metastases, indicating response, after three cycles, but the patient developed new bone metastases after 8 months (Fig. 4a,b).

Two patients classed as partial responders were treated with AZD5069 at 160 mg BD. The first had de novo metastatic prostate cancer with bone and lymph node metastases (Gleason score unknown) that progressed after docetaxel in the hormone-sensitive setting, and then progressed on abiraterone, enzalutamide, and docetaxel sequentially in the castration-resistant setting prior to trial entry (Extended Data Fig. 6). Baseline biopsy was $AR\text{-}V7^{+}$. Before trial entry, PSA doubled every 2 months, and a 41% increase in nodal disease occurred over 4 months. PSA fell by 84% (344 ng ml^{-1} to 55 ng ml^{-1}) and nodal disease decreased by 20% at nadir (3–4 months; Fig. 4c,d). Radiologic progression-free survival was 8 months. The second patient classed as a responder had de novo metastatic prostate cancer (Gleason 9) with bone-only metastases, received docetaxel for hormone-sensitive prostate cancer, and then progressed in multiple bone metastases while on enzalutamide shortly before trial entry. Baseline biopsy was $AR\text{-}V7^{-}$. PSA doubling time was 4 months. CTC count initially increased from 11 per 7.5 ml of blood to a peak of 39 per 7.5 ml of blood during cycle 1, and then transiently decreased to 0 per 7.5 ml of blood during cycle 4. The patient had a radiologic progression-free survival of 8 months; however, there was no PSA decrease (Fig. 4a, Extended Data Fig. 7a and Supplementary Table 5).

The patient classed as a partial responder treated with AZD5069 at 120 mg BD had mCRPC (Gleason 8) that progressed on enzalutamide, administered for 14 months, 2 years before trial entry and then after docetaxel both in the castration-resistant setting. The baseline biopsy was $AR\text{-}V7^{+}$. At trial entry, the patient had progressing bone metastases, and new supra and infra-diaphragmatic lymphadenopathy compressing the inferior vena cava, pelvic veins and lymphatics, causing lower limb and abdominal wall lymphoedema. PSA fell by 89% (98 ng ml^{-1} to 11 ng ml^{-1}) after 5 cycles and measurable disease reduced by 31%, with clinical improvement of lymphoedema; radiologic and clinical responses lasting 11 months (Fig. 4e).

The patient classed as a partial responder treated with AZD5069 at 80 mg BD had a relatively high drug exposure, with AUC_{last} and C_{max} comparable to those of patients treated at 160 mg BD, and grade 4 neutropaenia necessitating dose reduction. This patient had Gleason 8 mCRPC with bone metastases, which progressed on docetaxel, abiraterone and radium-223. The patient had new bone metastases and a PSA doubling time of 4 months. CTC count decreased from 9 per 7.5 ml at baseline to 1 per 7.5 ml of blood at cycle 2; CTC conversion was maintained for seven cycles. The PSA response criterion was not met and there was no measurable disease. This patient remained on trial for 16 months. On the basis of the response, toxicity and

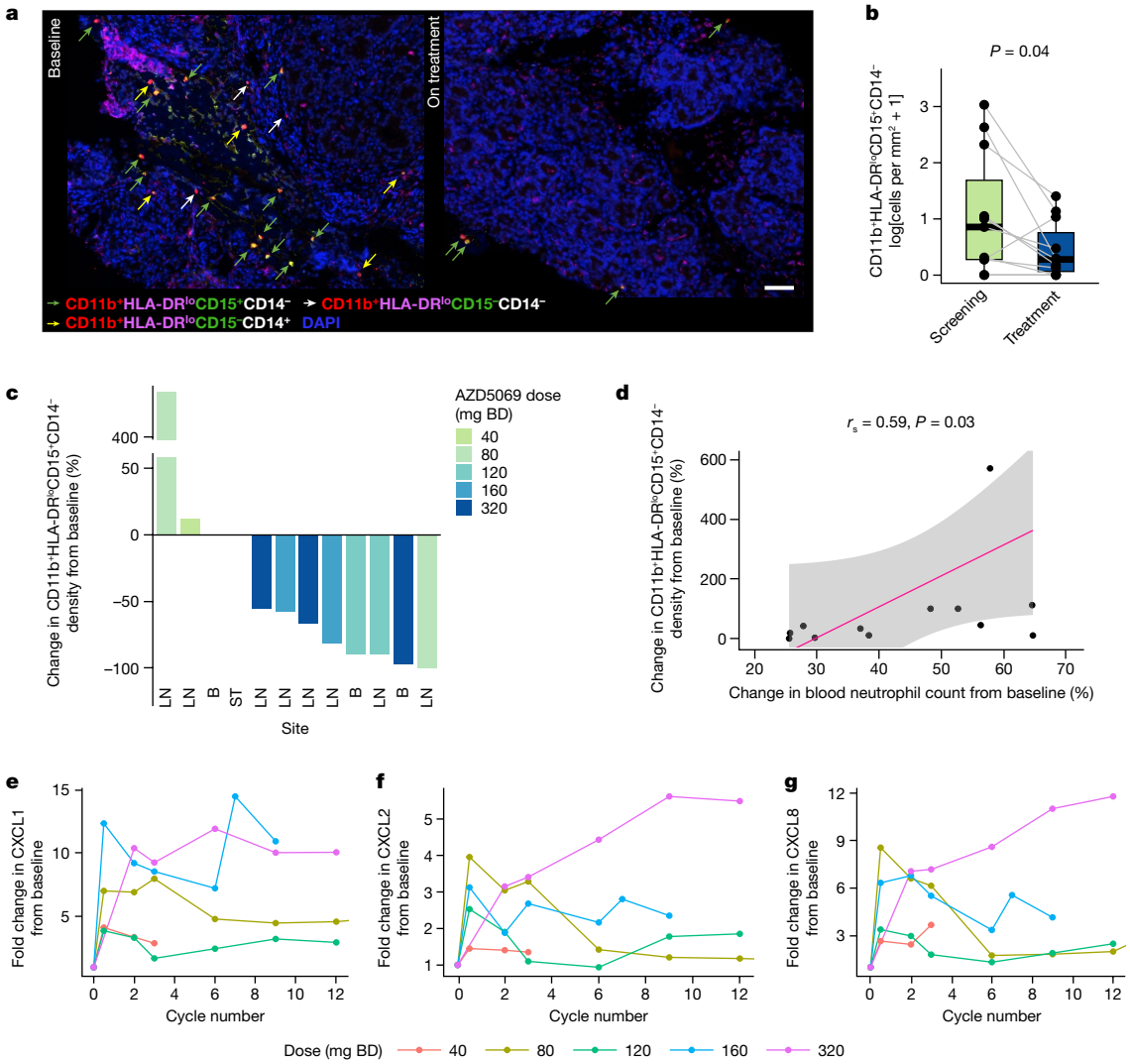

Fig. 3 | CXCR2 blockade reduces myeloid infiltration in some patients with CRPC. a, Example of a pair of CRPC biopsies showing myeloid cell changes before and after starting treatment. Green arrow: $CD11b^+HLA\text{-}DR^{lo}CD15^+CD14^-$ cells; yellow arrow: $CD11b^+HLA\text{-}DR^{lo}CD15^-CD14^+$ cells; white arrows: $CD11b^+HLA\text{-}DR^{lo}CD15^-CD14^-$ cells. Nuclei were counterstained with DAPI. Scale bar, 100 µm. **b**, Comparison of $CD11b^+HLA\text{-}DR^{lo}CD15^+CD14^-$ myeloid cell densities (log-transformed cells per mm^2) in mCRPC biopsies pre-treatment and on treatment in patients with blood neutrophil decrease of >30% (>40 mg BD dose levels; $n = 11$ pairs). Data are presented individually and as boxplots in which the middle horizontal line is the median, the lower and upper hinges are the first and third quartiles, and the upper and lower whiskers extend from the hinge to the minimum and maximum values. Grey lines link results from paired same-patient samples. Two-sided paired Wilcoxon signed-rank test *P* value is shown. **c**, Waterfall plot of percentage change in the density of $CD11b^+HLA\text{-}DR^{lo}CD15^+CD14^-$ myeloid cells in mCRPC biopsies before and after CXCR2i. The biopsy sites are annotated as LN for lymph node, B for bone, and ST for soft tissue. **d**, Scatter plot of the percentage of blood neutrophils on cycle 2 day 1 compared with baseline and the percentage of intratumour $CD11b^+HLA\text{-}DR^{lo}CD15^+CD14^-$ cell density after CXCR2i compared with baseline (for **c**,**d**, $n = 13$, but note that one outlier for which myeloid cell density increased from a baseline of zero (fold change = infinity) is not shown on the graph). An estimated linear regression line (pink) with 95% confidence interval (grey band), and correlation coefficients and *P* values from the two-sided Spearman's rank correlation analyses, are shown. **e**–**g**, By-dose-level, mean fold change in circulating CXCL1 ($n = 14$ patients), CXCL2 ($n = 20$ patients) and CXCL8 ($n = 20$ patients) levels on study compared with baseline, pre-treatment levels. Data for patients from whom samples were not collected, or whose samples failed quality control for enzyme-linked immunosorbent assay, are not included. Line colour indicates AZD5069 dose.

pharmacokinetic–pharmacodynamic associations, we recommended both the 160 mg BD and 320 mg BD dose levels for phase 2 evaluation; however, the expansion study was terminated owing to discontinued production of AZD5069.

To explore potential biomarkers of response, we compared the baseline molecular and immunologic profiles of patients classed as partial responders with those of patients classed as non-responders. This analysis showed no significant difference in baseline NLR, neutrophil count, lymphocyte count or the density of tumour myeloid, T and B cells, although only three patients classed as responders had biopsies for IF (Extended Data Fig. 7b–e). Patients classed as partial responders had lower on-treatment mean blood neutrophil counts compared with patients classed as non-responders (Fig. 4f,g). Varying degrees of increasing neutrophil counts were observed in patients classed as responders at progression (Fig. 2c and Extended Data Fig. 3).

We also examined CXCR2 expression on tumour cells, although this was rare in this cohort selected for adenocarcinoma tumour histology. In two of three of the patients classed as partial responders, CXCR2 protein was not detected on tumour cells at baseline. In one patient classed as a partial responder, CXCR2 was detected on 2.1%

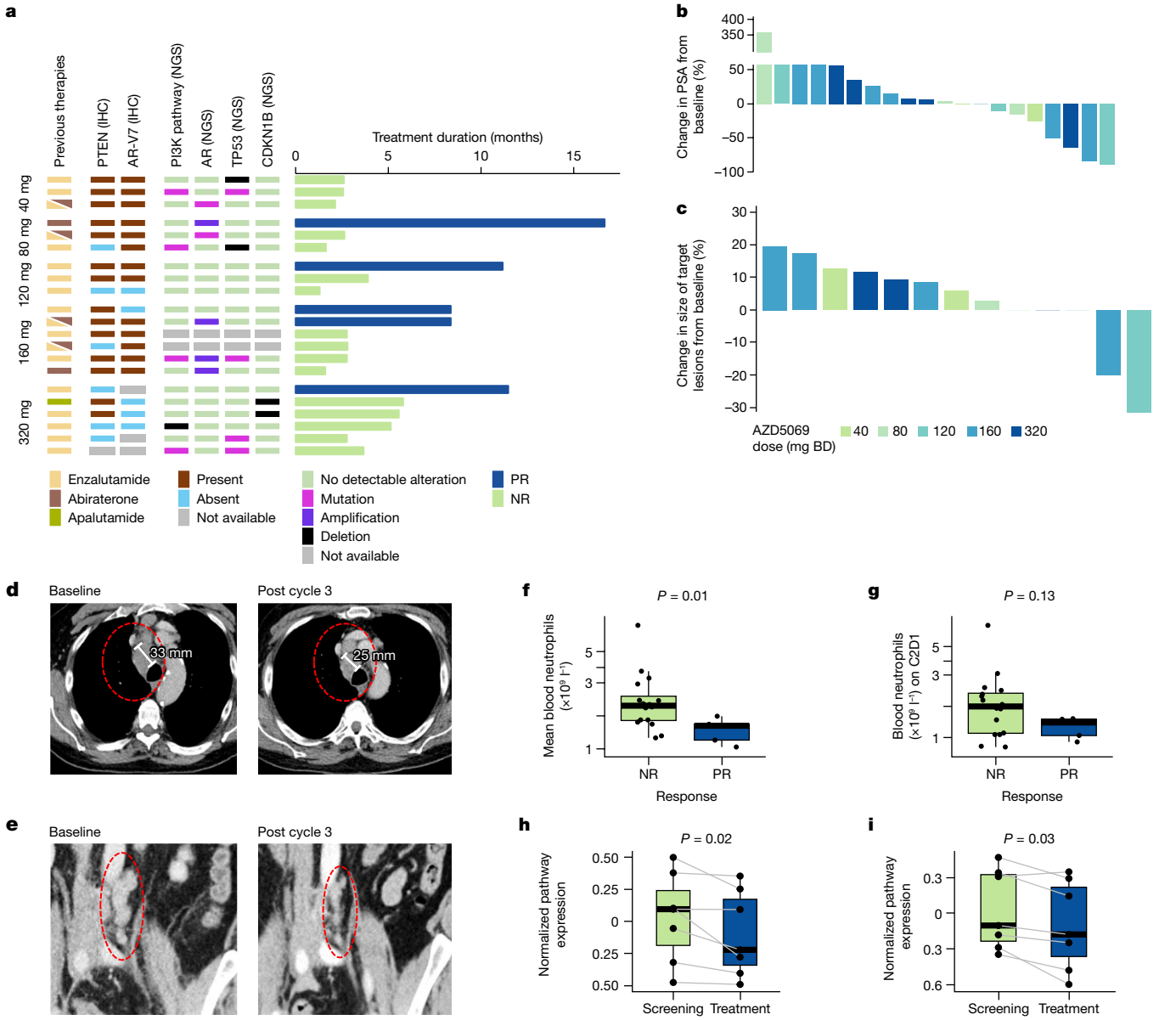

Fig. 4 | CXCR blockade can reverse ARSI resistance in patients with mCRPC. **a**, Treatment duration of response-evaluable patients grouped by AZD5069 dose ($n = 21$). Blue, patient classed as a partial responder; green, patient classed as a non-responder. Legend and coloured tiles indicate previous ARSI: enzalutamide (yellow), abiraterone (brown), apalutamide (dark green); AR-V7 protein status: nuclear Histo-score (HS) ≥ 10 (brown), nuclear HS < 10 (blue); PTEN protein status: nuclear or cytoplasmic HS ≥ 10 (brown), nuclear and cytoplasmic HS < 10 (blue), not available (grey); *TP53*, *AR* and *PTEN–PI3K* pathway genes, and *CDKN1B* genomic aberration status: no detectable alteration (green), pathogenic mutation (magenta), amplification (purple) and deletion (black) in baseline biopsies or cell-free DNA. **b**, Best PSA responses ($n = 20$). One patient was not evaluable for PSA response owing to early clinical disease progression. **c**, Best radiologic response in patients with measurable disease ($n = 13$). **d**,**e**, Example computerized tomography scan images of measurable disease taken pre-treatment and on treatment in two patients classed as partial responders treated at AZD5069 160 mg BD (**d**) and AZD5069 120 mg BD (**e**). White bars in **d** demarcate the short axis of a lymph node metastasis. **f**,**g**, Boxplots of mean blood neutrophil counts on treatment (**f**) and cycle 2 day 1 (C2D1) neutrophil counts (**g**) in patients classed as partial responders ($n = 5$) versus those classed as non-responders ($n = 16$). In **f**,**g**, data are presented individually and as boxplots in which the middle horizontal line is the median, the lower and upper hinges are the first and third quartiles, and the whisker extends from the hinge to the largest and smallest values no further than 1.5 × interquartile range (IQR) from the hinge. Two-sided Mann–Whitney *U*-test *P* values are shown. **h**,**i**, Expression of AR activity (**h**) and AR-V7 mRNA signatures (**i**) in same-patient pre- and on-treatment tumour biopsies ($n = 7$ pairs) with myeloid count decrease. In **h**,**i**, data are presented individually and as boxplots for which the middle line is the median, the lower and upper hinges are the first and third quartiles, and the upper and lower whiskers extend from the hinge to the maximum and minimum values. Grey lines link same-patient, paired samples. Two-sided paired Wilcoxon signed-rank test *P* values are shown.

of pan-CK$^+$CgA$^-$Syn$^-$CD56$^-$ cells and 1.8% of pan-CK$^+$ cells expressing at least one of the neuroendocrine phenotype markers. There was no significant change in the proportion of neuroendocrine phenotype marker-positive tumour cells overall or in the patients classed as partial responders (Extended Data Fig. 7f).

Given previous reports of CXCR2 chemokine upregulation in PTEN-deleted prostate tumours[10,11,20,23], we interrogated pre-treatment tumour PTEN protein expression (5 patients classed as partial responders, 15 patients classed as non-responders) and pathway gene alteration using a previously described next-generation sequencing (NGS)

panel[38] (5 patients classed as partial responders, 14 patients classed as non-responders). One patient classed as a responder had PTEN protein loss and eight patients classed as non-responders had PTEN protein loss or pathway-activating genomic alterations (Fig. 4a). We next evaluated genomic aberrations in cell cycle and senescence machinery genes (*CDKN1A*, *CDKN1B*, *CDKN2A*, *CDKN2B*, *CDKN2D, RB1* and *TP53*) using the aforementioned NGS panel on the basis of the hypothesis that myeloid-targeted approaches may depend on cell arrest and associated senescence programs in tumour cells for response. Alterations of these genes were not detected in the patients classed as partial responders, whereas 8/14 patients classed as non-responders had tumours with deep deletion or pathogenic mutation of *TP53* and *CDKN1B* (p27; Supplementary Table 6). These data indicate that the benefit of CXCR2 inhibition in mCRPC is not limited to tumours in which the PTEN–PI3K pathway is activated, but whether deleterious alterations in *TP53* or cyclin-dependent kinase (CDK) inhibitors confer resistance warrants further evaluation.

Impact of myeloid chemotaxis inhibition on tumour

To explore how CXCR2 inhibition of myeloid cell chemotaxis impacted mCRPC biology, we carried out capture-based RNA profiling (HTG EdgeSeq) from paired pre- and on-treatment mCRPC biopsies (seven pairs of biopsies had sufficient tumour content) from the patients with reduced intratumour $CD11b^{+}HLA\text{-}DR^{lo}CD15^{+}CD14^{-}$ myeloid cell density after treatment. We focused on the following: AR activity signatures[39]; AR-V7 signatures[40]; the IL-23 pathway signature[41]; and IL-6–JAK2–STAT3 signalling signatures[42]. CXCR2 blockade associated with downregulated AR activity and AR-V7 signatures, but did not associate with significant changes in the other pathways examined (Fig. 4h,i and Extended Data Fig. 7g,h). The degree of AR activity and AR-V7 signature downregulation was the most marked in the patient classed as a responder. AR activity and AR-V7 signature expression did not change significantly in patients in whom the density of intratumour $CD11b^{+}HLA\text{-}DR^{lo}CD15^{-}CD14^{-}$ cells did not decrease. Overall, these data support previous reports of myeloid infiltrates impacting oncogenic AR signalling.

Discussion

Myeloid inflammatory cells have been reported to play a key role in cancer therapy resistance and progression in preclinical models[10–12,14,15], but this has not been demonstrated in patients, with the drivers of intratumour myeloid infiltration remaining incompletely understood. This translational study demonstrates the relationship between peripheral and intratumour granulocytic myeloid compartments in patients with mCRPC, and indicates that a tumour-elicited and senescence-associated secretome drives CXCR2-expressing myeloid cell chemotaxis into tumour to fuel disease progression and treatment resistance. This is in keeping with preclinical studies showing that tumour cells, whether triggered by oncogenic signalling or treatment, sometimes in the context of senescence, can upregulate ligands that chemoattract myeloid cells[10,12,14,15,21]. The associations between NLR and neutrophil counts and high intratumour $CD11b^{+}HLA\text{-}DR^{lo}CD15^{+}CD14^{-}$ myeloid infiltration suggest that this simple blood test reflects a high level of intratumour myeloid cell infiltration into mCRPC. To our knowledge, this is the first clinical trial to show that CXCR2 blockade can reverse ARSI resistance to impart durable, clinical benefit in a subset of patients with CRPC. These data support the pathogenic role of myeloid inflammation in human prostate cancer and may explain why, across many cancer types, neutrophilia predicts worse outcome.

The responses in this study are probably mediated by tumour-extrinsic mechanisms given that few tumour cells expressed significant levels of CXCR2 protein, with the recruited patients having adenocarcinoma histology for which CXCR2 expression is rare[43]. The durable responses were unlikely to be due to re-response to enzalutamide monotherapy because patients either were progressing on enzalutamide immediately before trial entry or, if there was a treatment gap between trial entry and last ARSI, had tumours that expressed AR-V7, which associates with ARSI resistance[37]. The association between the degree of neutropaenia following CXCR2 blockade—a pharmacodynamic biomarker correlating with intratumour myeloid count decreases—and response suggests that myeloid cell clearance is critical to response. The downregulation of AR activity and AR-V7 signatures in tumours in which $CD11b^{+}HLA\text{-}DR^{lo}CD15^{-}CD14^{-}$ cell density decreased after treatment with CXCR2i is consistent with preclinical work showing that PMN-MDSCs drive AR signalling through IL-23, although PMN-MDSCs can make other paracrine factors including IL-6 and NRG1 (refs. 10,17). This array of ligands and metabolites can, however, impact several oncogenic and immunomodulatory pathways[10,12,14,44], and the observed downregulation of AR target genes could be indirect.

Several patients classed as non-responders had deleterious alterations of *TP53* and *CDKN1B*, alterations not detected in patients classed as partial responders; p53 and p27 loss may allow tumours to bypass cell cycle arrest[45,46]. Larger studies are needed to explore whether the wild-type status of tumour-suppressor genes associated with senescence including those expressing TP53 and CDK inhibitors predicts response to this therapeutic strategy. Elucidating resistance to this therapeutic strategy is also critically important; this may be due to incomplete intratumour myeloid cell clearance, or myeloid cell re-accumulation due to compensatory chemokine ligand upregulation, as was indicated by serial assessments of CXCR2 chemokines in our study, with some of the upregulated chemokines potentially binding not only CXCR2 but also CXCR1 (ref. 47). Understanding of these interactions, and the post-translational modifications that impact binding affinity and signalling, is now needed to elucidate the necessity of targeting multiple chemokine receptors to maximally block myeloid chemotaxis into tumours[48,49].

In conclusion, we provide evidence that CXCR2 blockade inhibits senescence-associated, tumour-elicited myeloid inflammation, with this blockade reversing ARSI resistance to confer durable antitumour activity in a subset of patients with mCRPC. Myeloid targeting warrants evaluation in larger cohorts of patients with prostate cancer and in earlier disease stages. Due consideration should be given to potential resistance mechanisms including redundant and compensatory chemokine–receptor interactions. The importance of this SASP biology to resistance to other senescence-inducing treatments also needs to be evaluated across treatments and cancer types.

Online content

Any methods, additional references, Nature Portfolio reporting summaries, source data, extended data, supplementary information, acknowledgements, peer review information; details of author contributions and competing interests; and statements of data and code availability are available at https://doi.org/10.1038/s41586-023-06696-z.

1. Hanahan, D. Hallmarks of cancer: new dimensions. *Cancer Discov.* **12**, 31–46 (2022).
2. Templeton, A. J. et al. Simple prognostic score for metastatic castration-resistant prostate cancer with incorporation of neutrophil-to-lymphocyte ratio. *Cancer* **120**, 3346–3352 (2014).
3. Leibowitz-Amit, R. et al. Clinical variables associated with PSA response to abiraterone acetate in patients with metastatic castration-resistant prostate cancer. *Ann. Oncol.* **25**, 657–662 (2014).
4. Valero, C. et al. Pretreatment neutrophil-to-lymphocyte ratio and mutational burden as biomarkers of tumor response to immune checkpoint inhibitors. *Nat. Commun.* **12**, 729 (2021).
5. Howard, R., Kanetsky, P. A. & Egan, K. M. Exploring the prognostic value of the neutrophil-to-lymphocyte ratio in cancer. *Sci. Rep.* **9**, 19673 (2019).
6. Sung, H. et al. Global cancer statistics 2020: GLOBOCAN estimates of incidence and mortality worldwide for 36 cancers in 185 countries. *CA Cancer J. Clin.* **71**, 209–249 (2021).
7. Beer, T. M. et al. Randomized, double-blind, phase III trial of ipilimumab versus placebo in asymptomatic or minimally symptomatic patients with metastatic chemotherapy-naive castration-resistant prostate cancer. *J. Clin. Oncol.* **35**, 40–47 (2017).

8. Kwon, E. D. et al. Ipilimumab versus placebo after radiotherapy in patients with metastatic castration-resistant prostate cancer that had progressed after docetaxel chemotherapy (CA184-043): a multicentre, randomised, double-blind, phase 3 trial. *Lancet Oncol.* **15**, 700–712 (2014).
9. Antonarakis, E. S. et al. Pembrolizumab for treatment-refractory metastatic castration-resistant prostate cancer: multicohort, open-label phase II KEYNOTE-199 study. *J. Clin. Oncol.* **38**, 395–405 (2020).
10. Calcinotto, A. et al. IL-23 secreted by myeloid cells drives castration-resistant prostate cancer. *Nature* https://doi.org/10.1038/s41586-018-0266-0 (2018).
11. Garcia, A. J. et al. Pten null prostate epithelium promotes localized myeloid-derived suppressor cell expansion and immune suppression during tumor initiation and progression. *Mol. Cell. Biol.* **34**, 2017–2028 (2014).
12. Di Mitri, D. et al. Tumour-infiltrating Gr-1^{+} myeloid cells antagonize senescence in cancer. *Nature* **515**, 134–137 (2014).
13. Guo, C. et al. CD38 in advanced prostate cancers. *Eur. Urol.* **79**, 736–746 (2021).
14. Lopez-Bujanda, Z. A. et al. Castration-mediated IL-8 promotes myeloid infiltration and prostate cancer progression. *Nat. Cancer* **2**, 803–818 (2021).
15. Wang, G. et al. Targeting YAP-dependent MDSC infiltration impairs tumor progression. *Cancer Discov.* **6**, 80–95 (2016).
16. Di Mitri, D. et al. Re-education of tumor-associated macrophages by CXCR2 blockade drives senescence and tumor inhibition in advanced prostate cancer. *Cell Rep.* **28**, 2156–2168 (2019).
17. Gil, V. et al. HER3 is an actionable target in advanced prostate cancer. *Cancer Res.* **81**, 6207–6218 (2021).
18. Wang, L. et al. A robust blood gene expression-based prognostic model for castration-resistant prostate cancer. *BMC Med.* **13**, 201 (2015).
19. Olmos, D. et al. Prognostic value of blood mRNA expression signatures in castration-resistant prostate cancer: a prospective, two-stage study. *Lancet Oncol.* **13**, 1114–1124 (2012).
20. Maxwell, P. J. et al. Potentiation of inflammatory CXCL8 signalling sustains cell survival in PTEN-deficient prostate carcinoma. *Eur. Urol.* **64**, 177–188 (2013).
21. Acosta, J. C. et al. Chemokine signaling via the CXCR2 receptor reinforces senescence. *Cell* **133**, 1006–1018 (2008).
22. Toso, A. et al. Enhancing chemotherapy efficacy in Pten-deficient prostate tumors by activating the senescence-associated antitumor immunity. *Cell Rep.* **9**, 75–89 (2014).
23. Armstrong, C. W. D. et al. Clinical and functional characterization of CXCR1/CXCR2 biology in the relapse and radiotherapy resistance of primary PTEN-deficient prostate carcinoma. *NAR Cancer* **2**, zcaa012 (2020).
24. Katoh, H. et al. CXCR2-expressing myeloid-derived suppressor cells are essential to promote colitis-associated tumorigenesis. *Cancer Cell* **24**, 631–644 (2013).
25. Highfill, S. L. et al. Disruption of CXCR2-mediated MDSC tumor trafficking enhances anti-PD1 efficacy. *Sci. Transl. Med.* **6**, 237ra267 (2014).
26. Cesano, A. nCounter®PanCancer Immune Profiling Panel (NanoString Technologies, Inc., Seattle, WA). *J. Immunother. Cancer* **3**, 42 (2015).
27. Fenor de la Maza, M. D. et al. Immune biomarkers in metastatic castration-resistant prostate cancer. *Eur. Urol. Oncol.* **5**, 659–667 (2022).
28. Proudfoot, A. E. I. Chemokine receptors: multifaceted therapeutic targets. *Nat. Rev. Immunol.* **2**, 106–115 (2002).
29. Eash, K. J., Greenbaum, A. M., Gopalan, P. K. & Link, D. C. CXCR2 and CXCR4 antagonistically regulate neutrophil trafficking from murine bone marrow. *J. Clin. Invest.* **120**, 2423–2431 (2010).
30. Matsusaka, T. et al. Transcription factors NF-IL6 and NF-kappa B synergistically activate transcription of the inflammatory cytokines, interleukin 6 and interleukin 8. *Proc. Natl Acad. Sci. USA* **90**, 10193–10197 (1993).
31. Stein, B., Cogswell, P. C. & Baldwin, A. S. Jr Functional and physical associations between NF-kappa B and C/EBP family members: a Rel domain-bZIP interaction. *Mol. Cell. Biol.* **13**, 3964–3974 (1993).
32. Burke, S. J. et al. NF-κB and STAT1 control CXCL1 and CXCL2 gene transcription. *Am. J. Physiol. Endocrinol. Metab.* **306**, E131–E149 (2014).
33. Alshetaiwi, H. et al. Defining the emergence of myeloid-derived suppressor cells in breast cancer using single-cell transcriptomics. *Sci. Immunol.* **5**, eaay6017 (2020).
34. Abida, W. et al. Genomic correlates of clinical outcome in advanced prostate cancer. *Proc. Natl Acad. Sci. USA* **116**, 11428–11436 (2019).
35. He, M. X. et al. Transcriptional mediators of treatment resistance in lethal prostate cancer. *Nat. Med.* **27**, 426–433 (2021).
36. Song, H. et al. Single-cell analysis of human primary prostate cancer reveals the heterogeneity of tumor-associated epithelial cell states. *Nat. Commun.* **13**, 141 (2022).
37. Antonarakis, E. S. et al. AR-V7 and resistance to enzalutamide and abiraterone in prostate cancer. *New Engl. J. Med.* **371**, 1028–1038 (2014).
38. Mateo, J. et al. DNA-repair defects and olaparib in metastatic prostate cancer. *N. Engl. J. Med.* **373**, 1697–1708 (2015).
39. Welti, J. et al. Targeting bromodomain and extra-terminal (BET) family proteins in castration-resistant prostate cancer (CRPC). *Clin. Cancer Res.* **24**, 3149–3162 (2018).
40. Sharp, A. et al. Androgen receptor splice variant-7 expression emerges with castration resistance in prostate cancer. *J. Clin. Investig.* **129**, 192–208 (2019).
41. Schaefer, C. F. et al. PID: the Pathway Interaction Database. *Nucleic Acids Res.* **37**, D674–D679 (2009).
42. Liberzon, A. et al. The Molecular Signatures Database (MSigDB) hallmark gene set collection. *Cell Syst.* **1**, 417–425 (2015).
43. Li, Y. et al. Targeting cellular heterogeneity with CXCR2 blockade for the treatment of therapy-resistant prostate cancer. *Sci. Transl. Med.* **11**, eaax0428 (2019).
44. Bronte, V. et al. Recommendations for myeloid-derived suppressor cell nomenclature and characterization standards. *Nat. Commun.* **7**, 12150 (2016).
45. Tonnessen-Murray, C. A., Lozano, G. & Jackson, J. G. The regulation of cellular functions by the p53 protein: cellular senescence. *Cold Spring Harb. Perspect. Med.* **7**, a026112 (2017).
46. Razavipour, S. F., Harikumar, K. B. & Slingerland, J. M. p27 as a transcriptional regulator: new roles in development and cancer. *Cancer Res.* **80**, 3451–3458 (2020).
47. Rajagopalan, L. & Rajarathnam, K. Ligand selectivity and affinity of chemokine receptor CXCR1. Role of N-terminal domain. *J. Biol. Chem.* **279**, 30000–30008 (2004).
48. Nasser, M. W. et al. Differential activation and regulation of CXCR1 and CXCR2 by CXCL8 monomer and dimer. *J. Immunol.* **183**, 3425–3432 (2009).
49. Moussouras, N. A. et al. Differences in sulfotyrosine binding amongst CXCR1 and CXCR2 chemokine ligands. *Int. J. Mol. Sci.* **18**, 1894 (2017).

Methods

Trial participants

We conducted an international, phase 1, multi-centre, single-arm, open-label trial (ClinicalTrials.gov identifier: NCT03177187, EudraCT: 2016-003141-28) at three centres in Europe (RMH (UK), Belfast City Hospital (UK), Oncology Institute of Southern Switzerland (Switzerland)). Eligible patients were consenting patients aged ≥18 years, who had mCRPC with histologically confirmed prostate adenocarcinoma histology, documented cancer progression at the time of trial entry by Response Evaluation Criteria in Solid Tumors (v.1.1) and/or Prostate Cancer Working Group 2 criteria, and PSA of ≥10 ng ml^{-1} at screening. Patients needed to have disease progression while on androgen deprivation therapy (orchiectomy and/or ongoing luteinizing hormone-releasing hormone (LHRH) agonist treatment), and confirmed disease progression on at least one of enzalutamide, darolutamide, apalutamide or abiraterone, having received at least 12 weeks of treatment of each. Before treatment with other prostate cancer treatments was permitted: patients needed to be undergoing androgen deprivation therapy with serum testosterone <50 ng dl^{-1} (<2.0 nM); patients needed to be Eastern Cooperative Oncology Group performance status of 0 or 1, and have adequate haematologic, renal, liver, and coagulation function; patients also needed to be willing to undergo pre- and on-treatment mCRPC biopsies, when safe and feasible.

Patients were excluded if their prostate cancer was predominantly small cell or neuroendocrine differentiated. Patients were excluded if they had any of the following: surgery, chemotherapy or other anticancer therapy (with the exception of an ARSI and gonadotropin hormone-releasing hormone analogue therapy) within 4 weeks before trial entry; limited field radiotherapy within 2 weeks or wide-field radiotherapy within 4 weeks of trial entry; hypoaldosteronism or hypopituitarism; history of seizures or predisposing factors to seizures; known central nervous system metastasis; malabsorption syndrome; prolonged QT interval > 470 milliseconds; clinically important rhythm, conduction, or ECG abnormality; predisposing factor to QT prolongation; coronary intervention, myocardial infarction, angina, or congestive cardiac failure (New York Heart Association ≥grade 2) in the past 6 months; uncontrolled hypotension or hypertension; clinically important history of liver disease (for example, Child–Pugh B or C, viral or other hepatitis, current alcohol abuse, or cirrhosis); malignancy other than prostate cancer within the past 5 years; immunocompromising disorder; thromboembolic event within the past 12 months; active or uncontrolled autoimmune disorder requiring steroids. Full eligibility criteria are described in the study protocol (Supplementary Information).

Study oversight

The study was conducted in accordance with the provisions of the Declaration of Helsinki and Good Clinical Practice guidelines. Regulatory approvals were obtained from the Medicines Healthcare products Regulatory Agency, Swiss Swissmedic and the institutional research ethics committee (REC; the London-Surrey Borders REC (UK sites) and Comitato Etico Cantonale Bellinzona (Switzerland)). Written informed consent was obtained from all participants. No participant compensation was provided. A safety review committee evaluated the safety and tolerability at regular intervals after recruitment of three patients to a schedule. All protocol amendments were approved by the trial sponsor, Medicines Healthcare products Regulatory Agency, Swissmedic and local UK and Swiss RECs. The study was sponsored and monitored by The Institute of Cancer Research (ICR), UK. The study was registered on ClinicalTrials.gov before commencement.

Study design

In this investigator-initiated, international, open-label, phase 1 study, we evaluated five escalating doses of orally administered AZD5069 (40 mg BD, 80 mg BD, 120 mg BD, 160 mg BD and 320 mg BD) in combination with standard, fixed-dose, orally administered enzalutamide (160 mg OD), over 28-day cycles, until disease progression, intolerance or withdrawal of consent. During the first cycle (42 days), AZD5069 was commenced 2 weeks before enzalutamide in the first four cohorts, primarily to evaluate any pharmacokinetic interactions between the two drugs. The starting dose of AZD5069 was determined on the basis of preclinical pharmacokinetics results as well as pharmacodynamic, pharmacokinetic and safety results from previous studies in humans in which the main side effect observed was dose-dependent, reversible neutropaenia in blood, without significant increase in infection rate in patients with airway disease, or healthy individuals.

The dose-escalation phase used a rule-based 3 + 3 design, with an initial three patients enrolled per dose level. If none of the first three patients experienced a DLT, dose escalation proceeded to the next dose level. If one instance of DLT was observed in three patients, up to six patients were treated at that dose level. If fewer than two of six patients at any dose level experienced a DLT, dose escalation continued to the next level. If at least two out of up to six patients experienced a DLT, dose escalation stopped and this dose level was defined as the maximum administered dose. Once this maximum administered dose was defined, the maximum tolerated dose (MTD) was confirmed at the dose level below the maximum administered dose. At least six evaluable patients were required to establish the MTD at a specific dose level. Only doses at which no more than one of six patients had a DLT could be defined as the MTD. Four potential dose-escalation cohorts with increasing AZD5069 doses (40 mg BD, 80 mg BD, 120 mg BD and 160 mg BD) were planned initially. The study protocol was amended on 16 December 2020 to explore a fifth dose level of AZD5069, 320 mg BD, with the option to de-escalate to 240 mg BD (dose level 4B) if dose level five was intolerable, and the study drugs were administered concurrently. This amendment occurred after previous dose levels were deemed safe and because a decrease in AZD5069 exposure was observed after adding enzalutamide. Intra-patient dose escalation was not permitted. Start of dosing between the first and second patient enrolled to each dose level was staggered by 1 week. Once the MTD was determined in the phase 1 study, the recommended phase 2 dose was determined on the basis of available data, including but not limited to safety and response.

Study procedures

Safety monitoring. Adverse events were monitored at least weekly during cycles 1 and 2, and then once per cycle from cycle 3 onwards, and graded using the National Cancer Institute Common Terminology Criteria for Adverse Events (NCI-CTCAE) v.4.0, until 28 days after the discontinuation of study treatment or until the resolution of a persistent drug-related adverse event. DLTs were defined as described in the study protocol. Notably, febrile neutropaenia (neutrophil count $<0.5 \times 10^9$ l^{-1} and fever >38.3 °C or fever ≥38 °C for >1 h), infection with grade 4 neutropaenia, and grade 4 neutropaenia for 7 days or more were defined as DLTs. Prophylaxis with growth factor support or antipyretics were not permitted. Investigators determined whether an adverse event was related to the study drugs. If a patient experienced clinically significant and/or unacceptable toxicity, including a DLT, not attributable to the disease or disease-related processes, dosing was interrupted or the dose was reduced and supportive therapy was administered as required. If the toxicity resolved or reverted to ≤CTCAE v.4.0 grade 1 within 14 days of onset, treatment with the combination of enzalutamide and AZD5069 could be restarted following agreement with the sponsor.

In patients who experienced grade 3 or greater toxicity related to enzalutamide in the opinion of the investigator that could not be ameliorated by the use of adequate medical intervention, enzalutamide dosing was interrupted until the toxicity improved to grade 1 or lower severity, and a dose reduction to enzalutamide 120 mg daily was

permitted. No further dose reduction for enzalutamide was permitted. During dose interruption due to an adverse event deemed related to AZD5069, treatment could be recommenced at the same dose if the toxicity resolved or reverted to CTCAE v.4.0 grade ≤1 in less than eight days; however, if the toxicity took 8 to 14 days to resolve or revert to grade ≤1, AZD5069 could be restarted at a lower dose (one dose level lower than the last dose received) as per specification in the protocol. Enzalutamide dose remained unchanged. For all other events, if the toxicity did not resolve to CTCAE v.4.0 grade ≤1 after more than 14 days, then treatment was discontinued and the patient was observed until resolution of the toxicity. Patients were taken off study if either study drug had to be permanently discontinued.

Tumour response assessment. Radiologic tumour responses were measured by computerized tomography of the thorax, abdomen and pelvis, bone scan, and, where indicated, whole-body magnetic resonance imaging, at baseline, once every 3 cycles, and then at the end of treatment if this was more than 8 weeks since the last scan. PSA and CTC count were measured at baseline, and then on day 1 of every cycle, and at the end of treatment. CTC counts were analysed using previously described methods[38].

Pharmacokinetic and pharmacodynamic studies. Blood samples for pharmacokinetic analyses of AZD5069 and enzalutamide were collected and analysed from all patients in the first four dose levels at the commencement of AZD5069 (cycle 1 day −14), cycle 1 day 1 (after 2 weeks of AZD5069 monotherapy) and cycle 2 day 1 (after 4 weeks of AZD5069 and enzalutamide combination). Specific pharmacokinetic collection time points are listed in the study protocol. Pharmacokinetic parameters were calculated using non-compartmental analysis (Phoenix v.8.1, Certara). Fresh tumour needle core biopsies from matched disease sites (lymph node, bone and soft tissue) were collected at baseline (within 1 week of treatment commencement) and approximately 2 weeks after starting AZD5069 in patients when this was deemed safe and feasible. Tumour biopsies were obtained from 18 patients under computerized tomography or ultrasound guidance by an experienced interventional radiologist (N.T.). Three patients did not undergo biopsies because this was not deemed safe or the patient declined. One patient had only a baseline tumour biopsy. Two patients underwent on-treatment biopsies after 4 weeks. Immediately after biopsy, tumour samples were immersed in 10% neutral-buffered formalin for 24 hours. Samples were processed through paraffin wax for histologic examination. Three 3 µm sections of formalin-fixed paraffin-embedded (FFPE) tumour biopsy were stained with haematoxylin and eosin to confirm the presence of tumour by a pathologist (B.G.). Tumour samples with insufficient tumour content or significant crushed artefact were excluded from analyses (B.G.). Baseline FFPE samples were analysed by IHC, and pre- and post-treatment FFPE biopsies were analysed by IF and targeted RNA profiling using HTG EdgeSeq. All samples that failed initial analyses by IF were restained at least once. A list of tumour samples and their methods of analyses are detailed in Supplementary Table 4.

Outcomes

The primary endpoints were to identify the DLTs, estimate the MTD and identify the recommended phase 2 dose of AZD5069 administered in combination with enzalutamide at 160 mg OD. Secondary endpoints were:(i) the rate of objective response, with objective response defined as confirmed soft tissue objective response by Response Evaluation Criteria in Solid Tumors v.1.1 in those with measurable disease, and/or PSA decline ≥50% confirmed 4 weeks or later, and/or CTC count conversion from ≥5 per 7.5 ml of blood at baseline to <5 per 7.5 ml of blood at nadir; (ii) pharmacokinetic parameters, including maximum concentration, area under the concentration–time curve; and (iii) pharmacodynamic changes including identifying patients whose blood NLR, neutrophil, and intratumour myeloid cell density decrease. Exploratory endpoints included blood cytokine levels and evaluation of tumour molecular profile on response.

Patient samples for myeloid cell translational studies

The association between myeloid cell densities and NLR was evaluated in two cohorts (Supplementary Table 1). Cohort 1 consisted of 48 mCRPC biopsies from patients treated at ICR/RMH, Oncology Institute of Southern Switzerland and Belfast City Hospital between 2012 and 2021. All patients provided informed consent, and enrolled onto institutional protocols approved by the local RECs (REC reference: 04/Q0801/60, 11/LO/2019). The validation cohort consisted of 57 mCRPC biopsies from patients treated at ICR/RMH between 2012 and 2016 under institutional protocols approved by the local REC (REC references: 04/Q0801/60, 2017-01002 CE TI 3237). Full blood counts were carried out using routine automated haematology analysers. NLR was defined as the quotient of the absolute peripheral blood neutrophil count divided by the absolute blood lymphocyte count. For comparisons of peripheral blood NLR with intratumour myeloid cell density, blood counts collected on the day of the biopsy, or when this was not available, within 7 days preceding the biopsy were used. Human biological samples were sourced ethically and their research use was in accordance with the terms of the informed consent provided. Studies of CXCR2 expression on immune cells and tumour cells consisted of 14 patients treated at the RMH who underwent mCRPC biopsies under a research protocol approved by The RMH REC (REC reference: 04/Q0801/60) providing consent for these analyses.

IF and IHC

Antibody validation. Antibodies against CXCR2, FOXP3, MUM1, CD163, CD68, HLA-DR, CD4, CD38, CD206, CD8 and GzB were validated by western blot and/or IHC comparing detection of protein expression in cells treated with either non-targeting control siRNA or ON-TARGETplus pooled siRNA against the target gene (Dharmacon) or using positive and negative control cell lines. Cells were authenticated by STR profiling and tested for mycoplasma (Venor GeM Mycoplasma Detection Kit, Minerva Biolabs). Markers were validated for appropriate tissue localization on immunohistochemical staining of relevant positive and negative tissue controls and reviewed by a certified pathologist (B.G.). Validation for PTEN, CD4, CD8, FOXP3, CD11b, CD15, CD14, CD138, CD20, Syn, CgA and AR-V7 was also previously described[13,17,50,51]. IHC was carried out on FFPE tissue sections using an automated staining platform (Bond RX, Leica Biosystems). Bone biopsies were decalcified using pH 7 EDTA for 48 h at 37 °C. Once validated for target sensitivity and specificity, the antibodies were further optimized for IHC, multiplex IF and hyperplex IF using methods described below. The full list of antibodies, working dilutions and incubation times is in Supplementary Tables 7 and 8.

Hyperplex IF assay. FFPE CRPC biopsies were stained using a hyperplex IF assay. For paired samples, the pre- and on-treatment biopsies from each patient, along with the positive and negative controls (tonsil, ovarian cancer, appendix, HeLa and LNCaP cell line pellet), were placed on the same slide to control for any technical variability in staining intensity and allow for comparison of the pre- and on-treatment biopsies. Samples from the tissue microarrays had been stained previously using orthogonal methods (IF and/or IHC) for confirmation. Standard operating procedures were implemented to control for known factors that can impact IF staining intensity, including the use of antibodies with the same lot number, minimization of freeze–thaw of antibodies, and controlling for the temperature of the experiment. Automated hyperplex IF staining and imaging was carried out on the COMET platform (Lunaphore Technologies). Slides underwent iterative staining and imaging, followed by elution of the primary and secondary antibodies[52].

FFPE tissue sections of 3 µm in thickness were baked in an oven for 60 min at 60 °C, followed by deparaffinization in xylene and

rehydration in a series of ethanol solutions of decreasing concentrations. Next, tissue sections were fixed in 10% neutral-buffered formalin solution (No. BAF-0010-05A, CellPath) for 20 min at room temperature. Antigen retrieval was achieved by heating the slides in heat-induced epitope retrieval buffer H pH 9 (No. TA-999-DHBH, Epredia, Shandon Diagnostics) in the PT Module (No. A80400011, Thermo Fisher Scientific) for 60 min at 102 °C. Subsequently, slides were rinsed and stored in Multistaining Buffer (BU06, Lunaphore Technologies) until use.

The hyperplex IF protocol template was generated using the COMET Control Software (v.0.70.0.1, Lunaphore Technologies), and reagents were loaded onto the device to carry out the sequential IF (seqIF) protocol[52]. Secondary antibodies were used as a mix of two species' complementary antibodies plus DAPI, Alexa Fluor Plus 647 goat anti-rabbit (No. A32733, 1:400 dilution, Thermo Scientific) and Alexa Fluor Plus 555 goat anti-mouse (No. A32727, 1:200 dilution, Thermo Scientific) diluted in Intercept T20 (TBS) antibody diluent (No. 927-65001, LI-COR Biosciences). Nuclear signal was detected with DAPI (No. 62248, dilution 1:1,000, Thermo Fisher Scientific) by dynamic incubation of 2 min. Primary antibodies were diluted in multistaining buffer (BU06, Lunaphore Technologies). For each cycle, the following exposure times were used: DAPI 80 ms, TRITC 400 ms, Cy5 200 ms. The elution step lasted 2 min for each cycle and was carried out with elution buffer (BU07-L, Lunaphore Technologies) at 37 °C. The quenching step lasted for 30 seconds and was carried out with quenching buffer (BU08-L, Lunaphore Technologies). The imaging step was carried out with imaging buffer (BU09, Lunaphore Technologies). The seqIF protocol in COMET resulted in a multi-stack ome.tiff file in which the imaging outputs from each cycle are stitched and aligned. COMET ome.tiff contains a DAPI image, intrinsic tissue autofluorescence in TRITC and Cy5 channels, and a single fluorescent layer per marker.

Elution efficiency and epitope stability of each biomarker were assessed separately through several rounds of staining, elution and imaging on positive control tissue. Antibody titration was carried out to identify the best antibody dilution and incubation time. The staining sequence was optimized through an iterative process using several positive and negative FFPE controls (appendix, tonsil, ovarian cancer and prostate cancer), cell lines (PC3, LNCaP and HeLa) and a patient-derived xenograft with a neuroendocrine phenotype (CP142)[17]. Images were reviewed by a pathologist (B.G.) and used to determine the final marker permutation (Supplementary Table 7 and Supplementary Figs. 1 and 2).

Six-colour IF. Six-colour OPAL-based sequential IF staining was carried out on the Bond RX automated staining platform (Leica Biosystems). FFPE tissue sections of 3 µm underwent heat-induced epitope retrieval with epitope retrieval solution 2 (pH 9.0; No. AR9640, ER2, Leica Biosystems) followed by endogenous peroxidase blocking (Novocastra Peroxidase Block, No. RE7157, Leica Biosystems) for 10 min. Nonspecific antibody binding was blocked using OPAL antibody diluent/block (ARD1001EA, Akoya Biosciences) for 10 min. Primary antibodies against CXCR2, CD15, CD11b, CD14 and HLA-DR; Supplementary Table 8) were sequentially incubated for 30 min followed by detection with the Novolink Max Polymer Detection System (RE7280-K, Leica Biosystems). IF signals for CXCR2, CD15, CD11b, CD14 and HLA-DR were visualized using TSA coumarin (NEL703001KT, Akoya Biosciences), OPAL 520 (NEL820001KT, Akoya Biosciences), OPAL 570 (NEL820001KT, Akoya Biosciences), OPAL 650 (FP1496001KT, Akoya Biosciences) and OPAL 780 (FP1501001KT, Akoya Biosciences), respectively, and counterstained with spectral DAPI. Slides were scanned using the VS200 Research Slide Scanner (Olympus).

AI-assisted image analyses. The hyperplex and six-colour IF assay images were reviewed by a certified pathologist (B.G.) and histopathologists (M.C., A.F., I.F.). Images were analysed using Halo software (Indica Labs). Tissue segmentation was carried out using a supervised machine learning algorithm to recognize prostate cancer foci and surrounding stroma. Cell segmentation was achieved with nuclear DAPI counterstain and tumour-infiltrating immune cells were phenotypically characterized by cell surface marker. We identified $CD11b^{+}HLA\text{-}DR^{lo}CD15^{+}CD14^{-}$ and $CD11b^{+}HLA\text{-}DR^{lo}CD15^{-}CD14^{+}$ cells using a supervised machine learning algorithm trained by a pathologist (B.G.) as previously described[13].

For the hyperplex IF panel, a threshold for positivity for each marker used for cell phenotyping was set by the pathologist by referencing positive and negative control tissue or cell line pellets stained on the same slide. The same thresholds were applied to the entire slide. Manual curation and comparison with controls was essential because differences in tissue type and quality can impact the intensity of different antibodies differently, although all phenotypic markers showed excellent signal-to-noise ratio (>15). Using these thresholds, Halo software (Indica Labs) was used to analyse each cell for the marker to provide single-cell-level binary readouts for phenotypic markers of interest. A Boolean gating strategy to identify cell types of interest on the basis of the intensity and specificity of markers was established (Supplementary Fig. 2).

Next-generation sequencing

Targeted NGS using a 113-gene panel was carried out on 16 available pre-treatment tumour biopsies, and 3 pre-treatment cell-free DNA samples, extracted from 20 ml of plasma collected in Streck tubes. NGS was carried out using previously described methods[38,53]. Libraries were constructed from 40 ng of cell-free DNA using a customized GeneRead DNAseq Mix-n-Match v.2 panel (Qiagen) and sequenced on the MiSeq Sequencer (Illumina). The somatic variant calls were manually inspected in the Integrative Genomics Viewer (v.2.16.1, Broad Institute). The sensitivity of NGS results from cell-free DNA analyses was assessed by carrying this assay out on three additional samples from the AZD5069 320 mg BD dose level for which NGS on tumour biopsy was also carried out and we confirmed that all pathogenic alterations detected in the tumour biopsy were also found in the cell-free DNA.

RNA profiling of FFPE tumour biopsies

RNA profiling of FFPE tumour biopsies collected before and after starting AZD5069 was carried out by HTG EdgeSeq (HTG Molecular Diagnostics) using the HTG human transcriptome panel containing 19,616 nuclease protection probes (NPPs), including 19,398 gene target-specific 50-nucleotide probes, 100 negative control probes, 92 probes for RNA controls established by the External RNA Control Consortium, 22 probes that measure gDNA and 4 positive control probes. The assay was carried out with a minimum of 11 mm^2 of FFPE tumour micro-dissected sections. The sections were lysed according to the manufacturer's instructions, and added to a 96-well plate on the HTG EdgeSeq Processor (HTG Molecular Diagnostics) on which a quantitative nuclease protection assay was carried out. The addition of DNA nuclease protection probes (NPPs) was automated and they were allowed to hybridize for 16 hours to the target mRNAs. The excess non-hybridized DNA probes and non-hybridized mRNA were removed by S1 digestion leaving only NPPs hybridized to mRNA. This produced a 1:1 ratio of DNA detection probes to mRNA targets present in the sample. Libraries were constructed by adding sequencing indices and molecular barcodes to the NPPs through polymerase chain reactions (PCR). After clean-up and quantification by quantitative PCR using the kit KAPA Library Quantification Kit Illumina platforms, the libraries were pooled and sequenced on the NextSeq 500 using a High Throughput 75-cycle v.2.5 kit (Illumina). FASTQ files were generated using BCL2FATSQ v.2.0 and raw count data were generated using HTG EdgeSeq Parser Software (v.5.3, HTG Molecular Diagnostics). Data were analysed using the HTG EdgeSeq Reveal analysis software. Several quality control metrics were carried out: QC0 (insufficient sample quantity or poor sample quality) with positive control probes >4% reads was marked as a failure; QC1 (insufficient read depth) with total aligned reads <7 million per sample was marked as a failure; QC2 (high background signal) with median $\log_{10}$

negative control probes >2 was marked as a failure; QC3 (incomplete digestion of gDNA by DNase) with median $\log_{10}$ gDNA control probes >1 was marked as a failure. Samples failing any of the quality controls were removed from the subsequent analysis. Differential gene expression between pre- and on-treatment samples was carried out using the HTG EdgeSeq Reveal DESeq2 analysis pipeline and R Software (v.4.2.3).

Circulating cytokine analyses

Serum samples were collected at baseline, on day 1 of every cycle, and on cycle 1 day 15. CXCL2, CXCL5, CXCL6, CXCL7 and CXCL8 were measured in patient serum (diluted 1:2 except for CXCL7, which was diluted 1:200), then analysed using R&D Systems Luminex discovery assays using the Luminex 200 and interpolated using a five-parameter logistic curve fit. CXCL1 was measured in neat patient serum using the R&D Systems human GROα Quantikine ELISA using the Perkin Elmer Envision 2103 Multilabel plate reader and interpolated using linear regression. The Luminex and ELISA assays were validated to good clinical practice compliance by The ICR and included quality control samples of serum, unspiked or spiked with recombinant protein standard, from healthy volunteer serum in every analytical run. A list of the ELISA reagents is provided in Supplementary Table 9.

Bioinformatics

mCRPC transcriptome analysis. A total of 159 mCRPC transcriptomes generated by the SU2C–PCF Prostate Cancer Dream Team[34] were downloaded and reanalysed. Only samples that had library preparation using polyA+ RNA isolation were used (that is, samples with library preparation carried out by capture methods were excluded). A total of 141 mCRPC transcriptomes had associated survival data available for survival analyses. A separate 95 mCRPC transcriptomes from patients treated at RMH/ICR were analysed[27]; 94 mCRPC transcriptomes were used for the survival analyses as survival data were not available from 1 patient. The SU2C–PCF transcriptomes were aligned to the human reference genome (GRCh37/hg19) using TopHat2 (v.2.0.7). Gene expression as fragments per kilobase of transcript per million mapped reads (FPKM) was calculated using Cufflinks (v.2.2.1). Unbiased interrogation of pan-immune genes[26] present in the RMH/ICR bulk RNA-seq datasets in relation to NLR was carried out. MDSC signatures were adapted from previously published signatures[10,33]. Associations were analysed using the two-sided Spearman's rank correlation test.

mCRPC biopsy RNA profiling. For mCRPC tumour biopsy RNA profiling, HTG EdgeSeq data were processed with the EdgeSeq processor and included multiple steps (parsing, quality control and normalization) with default settings. The normalized counts were transformed to $\log_2$[counts per million], which was used for downstream analysis. Gene set variation analysis (GSVA, R package GSVA v.1.4) was used for molecular signature analysis.

Single-cell transcriptomic analysis. Single-cell transcriptomic data from 15 mCRPC samples from 14 patients (https://www.nature.com/articles/s41591-021-01244-6)[35] and single-cell transcriptomic data from 11 patients with localized prostate cancer (https://www.nature.com/articles/s41467-021-27322-4)[36] were downloaded. Data were loaded into R Software (v.4.1.3). The raw counts from the localized prostate cancer data were log normalized. Both datasets were processed with Seurat (v.4.3.0) and underwent scaling, clustering, dimensional reduction and cell type assignment with SingleR (v.1.8.1) using the Blueprint ENCODE reference dataset from the celldex (v.1.4.0) library.

Statistics

Sample size was chosen pragmatically. According to the rule-based 3 + 3 design, which guided dose-escalation decisions, the cohort size was three patients and skipping of dose levels was not allowed. Patients who completed the DLT period or experienced a DLT during the DLT period were considered part of the evaluable population. Patients who received at least one dose of study drug were considered part of the safety population. To be evaluable for response, the patient must have met the eligibility criteria, received at least three cycles of trial medication, and have had baseline assessment of disease. Comparisons of baseline characteristics between patients classed as responders and those classed as non-responders were carried out using the two-sided Mann–Whitney *U*-test. Comparisons of paired pharmacokinetic and pharmacodynamic parameters were carried out using the two-sided paired Wilcoxon signed-rank test. Safety variables and pharmacokinetic and pharmacodynamic endpoints were summarized descriptively.

Immune cell densities and continuous gene expression data are presented descriptively as individual values, as well as violin plots or boxplots with median and interquartile range. All analysable areas on the entire slide were analysed. The two-sided Spearman's rank correlation test was used to estimate associations between continuous variables, two-sided Mann–Whitney *U*-test was used to test for differences between unpaired groups, and the two-sided paired Wilcoxon signed-rank test was used to test for differences between paired samples. The Kruskal–Wallis test was used to compare myeloid cell densities across multiple disease sites. Multivariable linear regressions were carried out to determine whether associations between NLR or neutrophil count and myeloid cell densities were impacted by biopsy site. The Maxstat method[54,55] determined gene expression cutoffs for survival analyses. Overall survival and progression-free survival were estimated using the Kaplan–Meier method. Between-group comparisons of survival curves were carried out using the log-rank test. Hazard ratios with 95% confidence intervals were calculated using Cox regression. All P values ≤ 0.05 were considered significant. Bonferroni correction was applied to adjust for multiplicity in the context of multiple hypothesis testing of myeloid gene signatures but not for associations between NLR and immune genes for which the aim of the analyses was to identify the most highly ranked immune genes associating with NLR. Circulating cytokine levels are presented descriptively. Statistical analysis was carried out using R software (v.4.2.2) and according to the statistical analysis plan for trial-related analyses.

Reporting summary

Further information on research design is available in the Nature Portfolio Reporting Summary linked to this article.

Data availability

The full study protocol is provided in the Supplementary Information. Bulk RNA-seq data from the SU2C–PCF cohort[34] were downloaded from https://www.cbioportal.org/study/summary?id=prad_su2c_2019. Single-cell transcriptomic data from 15 mCRPC samples (https://www.nature.com/articles/s41591-021-01244-6) were downloaded from https://singlecell.broadinstitute.org/single_cell/study/SCP1244/transcriptional-mediators-of-treatment-resistance-in-lethal-prostate-cancer (study number SCP1244). Single-cell transcriptomic data from 11 patients with localized prostate cancer (https://www.nature.com/articles/s41467-021-27322-4) were downloaded from GEO accession GSE176031. De-identified, bulk RNA-seq data from the RMH cohort may be requested from the corresponding author (J.S.d.B.). Requests for the clinical and translational data from patient samples must provide clinically relevant rationale in adherence with the intent of the study and patients' consent, and will be reviewed by the corresponding author (J.S.d.B.) and the ICR to determine whether the request is subject to any intellectual property, ethical and/or confidentiality considerations. A prompt response will be provided to such requests. Patient identifiers or information that may reveal the patient's identity will not be shared. Any data or material that can be shared will be made available through a material transfer agreement with The ICR. Source data are provided with this paper.

50. Ferraldeschi, R. et al. PTEN protein loss and clinical outcome from castration-resistant prostate cancer treated with abiraterone acetate. *Eur. Urol.* **67**, 795–802 (2015).
51. Rescigno, P. et al. Characterizing CDK12-mutated prostate cancers. *Clin. Cancer Res.* https://doi.org/10.1158/1078-0432.Ccr-20-2371 (2020).
52. Migliozzi, D. et al. Microfluidics-assisted multiplexed biomarker detection for in situ mapping of immune cells in tumor sections. *Microsyst. Nanoeng.* **5**, 59 (2019).
53. Goodall, J. et al. Circulating cell-free DNA to guide prostate cancer treatment with PARP inhibition. *Cancer Discov.* **7**, 1006–1017 (2017).
54. Hothorn, T. & Lausen, B. On the exact distribution of maximally selected rank statistics. *Comput. Stat. Data Anal.* **43**, 121–137 (2003).
55. Lausen, B., Hothorn, T., Bretz, F. & Schumacher, M. Assessment of optimal selected prognostic factors. *Biom. J.* **46**, 364–374 (2004).

Acknowledgements We thank the patients and their families for participation in this study. The de Bono laboratory acknowledges funding from: Cancer Research UK (CRUK; CRM186x; CTRQQR-2021\1000009), Experimental Cancer Medicine Centre grant funding from CRUK and the Department of Health, and Biomedical Research Centre funding to the RMH, the Prostate Cancer Foundation (PCF) (19CHAL08), the US Department of Defense (W81XWH2110076), Prostate Cancer UK and the Movember Foundation through the London Movember Centre of Excellence (CEO13_2-002), National Institute for Health and Care Research (NIHR, NF-SI-0617-10099) and The V Foundation for Cancer Research (D2016-022). J.S.d.B. is an NIHR Senior Investigator. The views expressed in this article are those of the authors and not necessarily those of the National Health Service, the NIHR or the Department of Health. The ICR Clinical Trials and Statistics Unit receives programmatic infrastructure funding from CRUK (C1491/A25351). C.G. has been supported by the Wellcome Trust. A. Sharp has been supported by the Medical Research Council (MR/M018318/1) and PCF (18YOUN25), and is supported by the Wellcome Trust (219594/Z/19/Z) at present. D. Westaby is supported by CRUK (Clinical Research Training Fellowship). K.E.S. is financially supported by CRUK (CTRQQR-2021\100009). A.P. is supported by the PCF (20YOUN17). M.D.F. received grant funding from Fundación Cris contra el Cáncer. The Alimonti laboratory acknowledges funding from the Swiss-Card-Onco-Grant of Alfred and Annemarie von Sick, Swiss Cancer Research Foundation (KFS-5262-02-2021), the Swiss National Science Foundation (310030B_201274), Novartis Foundation, the US Department of Defense (W81XWH2110076), PCF (19CHAL08), the ISREC Foundation, Fondazione San Salvatore, Fondazione AIRC per la Ricerca sul Cancro (IG 22030) and the European Research Council (CoG 683136). J. Gil's laboratory is supported by the MRC (MC_U120085810) and CRUK (C15075/A28647). The clinical trial was sponsored by the ICR. AZD5069 was supplied by AstraZeneca, and enzalutamide was supplied by Astellas. The study received funding from Prostate Cancer UK (RIA15-ST2-018), Swiss-Card-Onco-Grant of Alfred and Annemarie von Sick, NIHR Biomedical Research Centre funding (BRC A148), Experimental Cancer Medicine Centre funding from CRUK and limited funding from AstraZeneca. The funders did not have a role in the study design; trial conduct; data collection, analyses and interpretation; writing of the report; or decision to submit the report for publication, with the exception of analyses of pharmacokinetic data. AstraZeneca was involved in the pharmacokinetic analyses of AZD5069, and Astellas was involved in the pharmacokinetic analyses of enzalutamide. AstraZeneca and Astellas reviewed the manuscript. All authors had full access to all study data and the corresponding author had final responsibility for the decision to submit for publication.

Author contributions J.S.d.B., A. Sharp, C.G., A.A., J. Gil and D. Waugh. conceived and/or designed the study. H.T., M.R., J.R. and C.Y. developed the statistical plan. J.R., M.R. and C.G. carried out the statistical analyses. J.R. and C.Y. supervised the statistical analyses. J.S.d.B. served as the chief investigator to the trial. S.J. and U.V. served as the principal investigators of the clinical trial. A. Sharp, C.G., C.T., A.P., K.C., R.C., C.A., M.D.F., D. Westaby, I.C., A. Stathis and N.T. served as co-investigators of the clinical trial. J.S.d.B., S.J., U.V., A. Sharp, C.G., C.T., A.P., K.C., R.C., C.A., M.D.F., D. Westaby, I.C., A. Stathis and N.T. recruited patients to, medically managed patients on, and/or collected data for the clinical trial. C.G., A. Sharp, J.C., M.D.F., D. Westaby and K.C. collected clinical data for the translational cohorts correlating NLR and neutrophils with myeloid cell densities. C.G., A.N., M.C., I.F., R. Riisnaes and A.F. carried out the antibody validation. M.C., I.F., R. Riisnaes and A.F. carried out the antibody optimization, IHC and multiplex IF assays. M.C., A.F., C.G., B.G. and A. Schlag established, optimized and/or carried out the hyperplex IF assay. B.G. annotated, segmented and gated the IF samples; B.G., C.G., G.S. and B.C. designed and/or carried out the downstream analyses. S.C., C.B. and J. Goodall carried out the NGS, RNA-seq and RNA profiling studies. L.G. carried out the single-cell RNA-seq analyses. W.Y. and D.B. carried out the bulk RNA-seq analyses. W.Y., S.C. and C.G. carried out the RNA profiling analyses. D.B. and C.G. carried out the survival analyses. R. Ruddle, F.R. and C.G. carried out the pharmacokinetic data analyses. K.E.S., J.M. and S.D. carried out the ELISA assays. K.E.S., J.M., S.D. and C.G. analysed the ELISA data. P.F. enumerated CTCs. R.M., H.B., T.P., A.T. and M.P. served as sponsors and monitored the study. C.G., J.S.d.B., A. Sharp, M.C. and S.C. wrote the manuscript. All authors provided advice on, reviewed, edited and approved the manuscript.

Competing interests A. Sharp, B.G., M.C., I.F., J.R., M.R., L.G., W.Y., S.C., K.C., A.P., C.B., G.S., J. Goodall, F.R., R. Ruddle, K.E.S., J.M., D.B., C.T., A.N., N.T., D. Westaby, J.C., M.D.F., C.Y., R.M., H.B., T.P., A.T., M.P., H.T., R. Riisnaes, A.F., P.F., S.D., A. Schlag and J.S.d.B. are employees of The ICR, which has a commercial interest in abiraterone, PARP inhibition in DNA-repair-defective cancers and PI3K–AKT pathway inhibitors. C.G. was an employee of The ICR during the conduct of this work, as well as submission, review, and revision of the manuscript, and is now an employee of Roche-Genentech. A. Sharp has received travel support from Sanofi, Roche-Genentech and Nurix, and speaker honoraria from Astellas Pharma and Merck Sharp & Dohme; has served as an advisor to DE Shaw Research and CHARM Therapeutics; and has been the chief or principal investigator of industry-sponsored clinical trials. J.S.d.B. has served on advisory boards and received fees from companies including Amgen, AstraZeneca, Astellas, Bayer, Bioxcel Therapeutics, Boehringer Ingelheim, Cellcentric, Daiichi, Eisai, Genentech/Roche, Genmab, GSK, Harpoon, Janssen, Merck Serono, Merck Sharp & Dohme, Menarini/Silicon Biosystems, Orion, Pfizer, Qiagen, Sanofi Aventis, Sierra Oncology, Taiho, Terumo and Vertex Pharmaceuticals. J.S.d.B. receives funding or other support for his research work from Daiich Sankyo, AstraZeneca, Astellas, Bayer, Cellcentric, Daiichi, Roche-Genentech, Genmab, GSK, Janssen, Merck Serono, MSD, Menarini/Silicon Biosystems, Orion, Sanofi Aventis, Sierra Oncology, Taiho, Pfizer and Vertex. J.S.d.B. was named as an inventor, with no financial interest, on US patent 8,822,438. J.S.d.B. has been the chief or principal investigator of many industry-sponsored clinical trials. S.J. has served on advisory boards and received fees from companies including Accord, AstraZeneca, Astellas, Bayer, Boston Scientific, Janssen and Pfizer; and reports research funding from Boston Scientific for other research projects. I.C. reports speaker, consultancy or advisory role activities for GSK, AstraZeneca, Novartis and MSD; travel grants from Tesaro, GSK, AstraZeneca and Janssen; and research funding (to institution as the principal investigator) from MSD, Bayer, Incyte, AstraZeneca and Vivesto. U.V. reports an advisory role (institutional) to Janssen, Astellas, Merck, MSD, Pfizer, Roche, Bayer, BMS and Novartis AAA; travel support from Janssen, Merck and Ipsen; being part of the speaker bureau for (compensated, institutional) Janssen, Astellas, Pfizer, Roche, SAMO, BMS and Ipsen; and grant funding from Fond'Action. A. Stathis serves as a principal investigator and receives institutional funding for clinical trials sponsored by AstraZeneca, Bayer, Incyte, Roche, Abbvie, ADC Therapeutics, Amgen, Cellestia, Loxo Oncology, Merck MSD, Novartis, Pfizer, Philogen and Roche; received travel grants from AstraZeneca and Incyte; served on advisory boards for Janssen and Roche; provided expert testimony to Bayer and Eli Lilly. M.D.F. received travel funding from Astellas, AstraZeneca, Pfizer, Pierre Fabre, Roche, Bristol Meiers Squibb, Novartis, MSD, Janssen and Bayer, and personal fees from Janssen, Pierre Fabre and Roche (all funding and fees were outside the submitted work). J. Gil has acted as a consultant for Unity Biotechnology, Geras Bio, Myricx Pharma and Merck KGaA. Pfizer and Unity Biotechnology have financially supported research in J. Gil's laboratory (unrelated to the work presented here). J. Gil owns equity in Geras Bio. J. Gil is a named inventor on MRC and Imperial College patents, both related to senolytic therapies (the patents are not related to the work presented here). A.A. has been the principal investigator of industry-sponsored clinical trials sponsored by Astellas Pharma Inc., AstraZeneca, Sun Pharma Global FZE; has received consulting fees from Debiopharm; and owns shares in Oncosence. B.C., D. Waugh., R.C. and C.A. do not have any competing interest to declare.

Additional information

Supplementary information The online version contains supplementary material available at https://doi.org/10.1038/s41586-023-06696-z.

Correspondence and requests for materials should be addressed to Johann S. de Bono.

Peer review information *Nature* thanks Ann Richmond, Adam Sowalsky and the other, anonymous, reviewer(s) for their contribution to the peer review of this work.

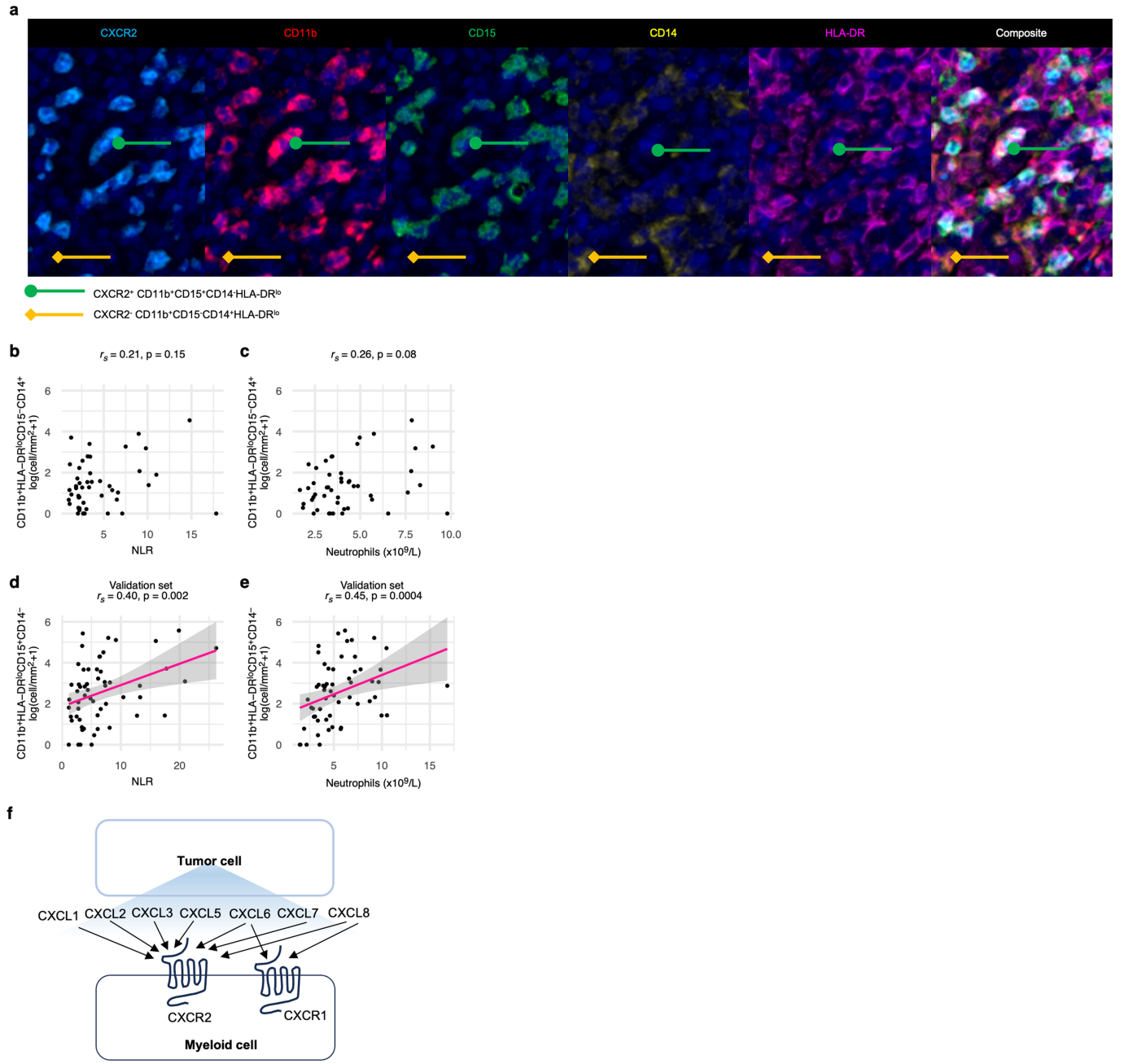

Extended Data Fig. 1 | Associations between CRPC myeloid cell density and NLR. a, Example images from the six-colour IF panel for identifying myeloid cells (example of staining of appendix) of CXCR2, CD15, CD11b, CD14, HLA-DR, and DAPI. Green pointer: CD11b$^+$HLA-DR^{lo}CD15$^+$CD14$^-$, yellow arrow: CD11b$^+$HLA-DR^{lo}CD15$^-$CD14$^+$. Scale bar = 20 µm. **b**,**c**, Scatter plot of peripheral blood NLR (**d**) and neutrophil count (x10^9/L) (**e**) versus log-transformed intratumor CD11b$^+$HLA-DR^{lo}CD15$^-$CD14$^+$ cell density (cells/mm^2) in cohort 1 (n = 48). **d**,**e**, Scatter plot of peripheral blood NLR (**b**) and neutrophil count (x10^9/L) (**c**) versus intratumor CD11b$^+$HLA-DR^{lo}CD15$^+$CD14$^-$ myeloid cell density (cells/mm^2) in the validation cohort (n = 57). For **a**–**e**, correlation coefficients and p-values from the two-sided Spearman's rank correlation analyses are shown. For **d**,**e**, estimated linear regression lines (pink) with 95% confidence interval (grey band). **f**, diagram of known CXCR1 and CXCR2 ligands. Source data are presented in the source data file.

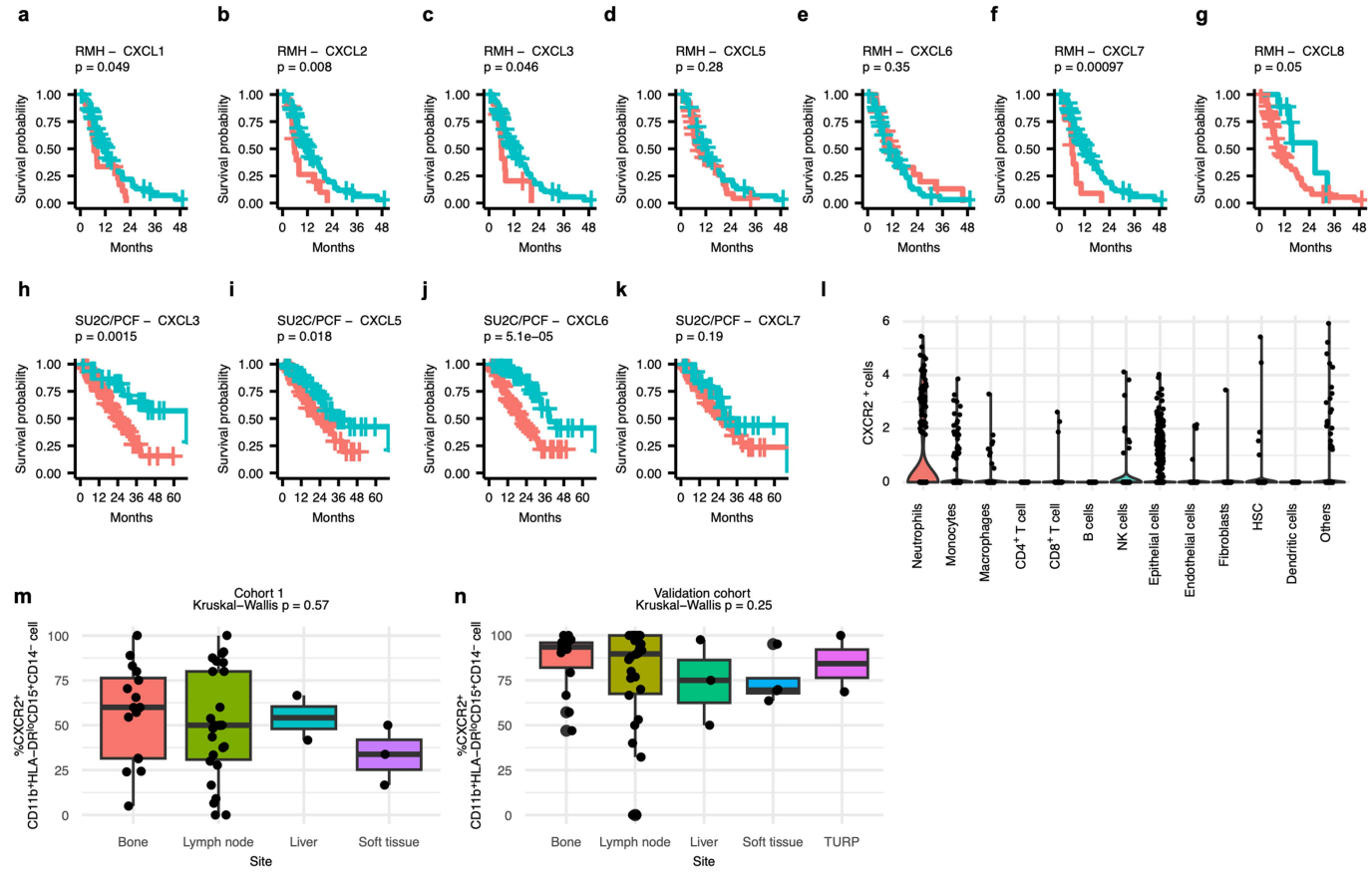

Extended Data Fig. 2 | Clinical relevance of targeting the CXCR2 axis on myeloid cells in CRPC. a–**k**, Kaplan-Meier curves showing survival of mCRPC patients from the time of CRPC biopsy based on gene expression of CXCR2 chemokines in the RMH cohort (n = 94) (**a**–**g**) and SU2C/PCF cohort (n = 141) (**h**–**k**). Gene expression cut-offs were determined using the Maxstat method. p-values were calculated using the log-rank test. For **(a**–**k)**, blue line represents low expression, red line represents high expression. **l**, Violin plot of CXCR2 mRNA expression on single cells from single-cell RNASeq data from 11 primary prostate tumour samples. **m**,**n**, Proportion of $CD11b^{+}HLA\text{-}DR^{lo}CD15^{+}CD14^{-}$ myeloid cells expressing CXCR2 by biopsy site in cohort 1 (n = 48) (**m**) and validation cohort (n = 57) (**n**). For m, n, data are presented individually and as boxplots where the middle line is the median, the lower and upper hinges are the first and third quartiles, the upper whisker extends from the hinge to the largest value no further than 1.5 × inter-quartile range (IQR) from the hinge and the lower whisker extends from the hinge to the smallest value at most 1.5 × IQR from the hinge. Kruskal-Wallis p-values comparing the percentage of $CXCR2^{+}$ myeloid cells across biopsy sites are shown. Source data for **a**–**k**, **m**,**n** are presented in the source data file.

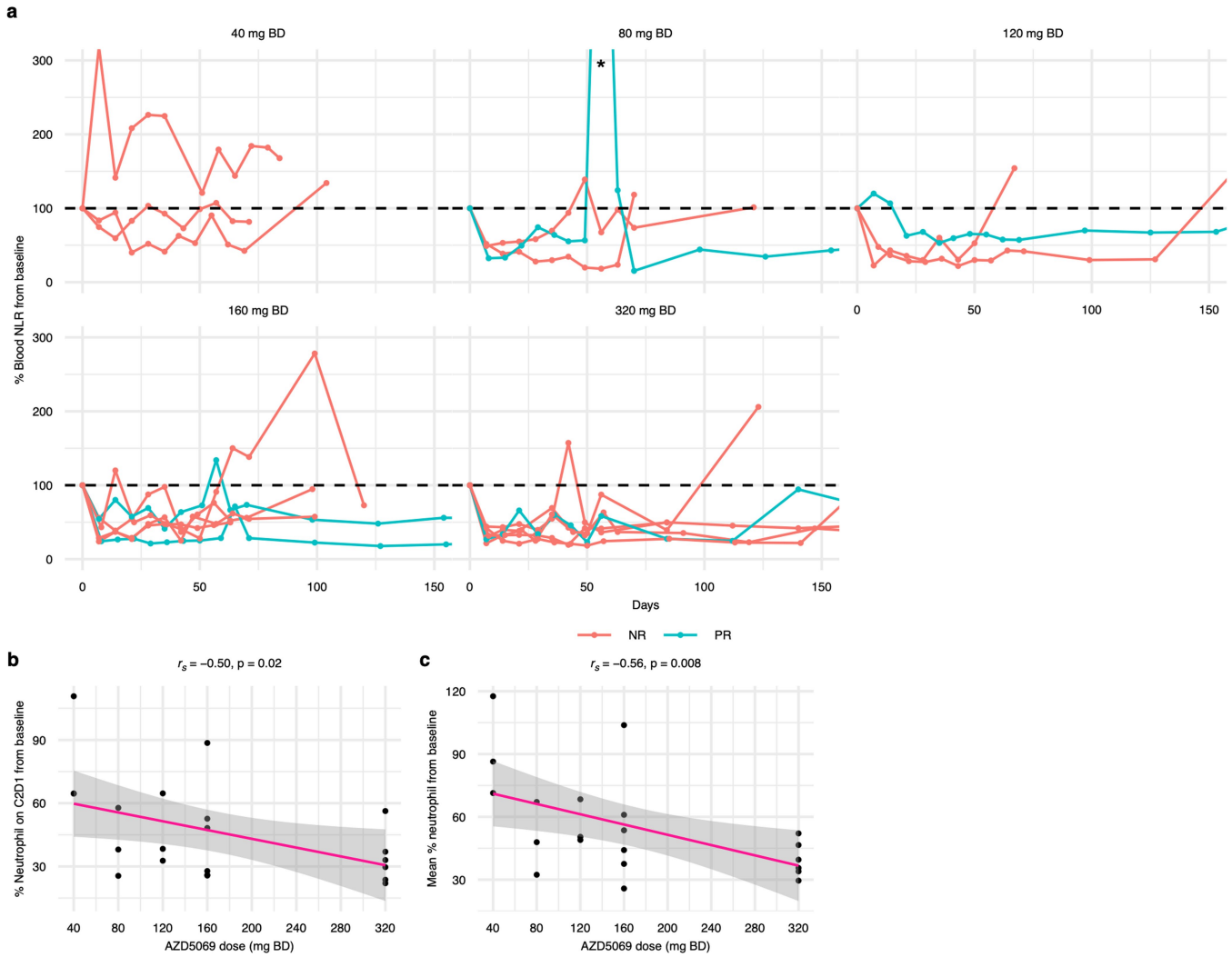

Extended Data Fig. 3 | CXCR2 inhibition led to dose-dependent decreases in blood neutrophils. a, By-patient, serial, peripheral blood NLR for each dose level of AZD5069. Aqua line: responder, Pink line: non-responder. *Outlier with NLR peak of 789% from baseline on cycle 2 day 15 in the setting of salmonella infection. **b**, Scatterplot of AZD5069 dose administered twice daily versus percentage peripheral blood neutrophil counts on cycle 2 day 1 compared with baseline. **c**, Scatterplot showing of AZD5069 dose versus mean percentage blood neutrophil count on treatment compared with baseline. For **b**,**c**, estimated linear regression lines (pink) with 95% confidence interval (grey band), and correlation coefficients and p-values from the two-sided Spearman's rank correlation analyses are shown.

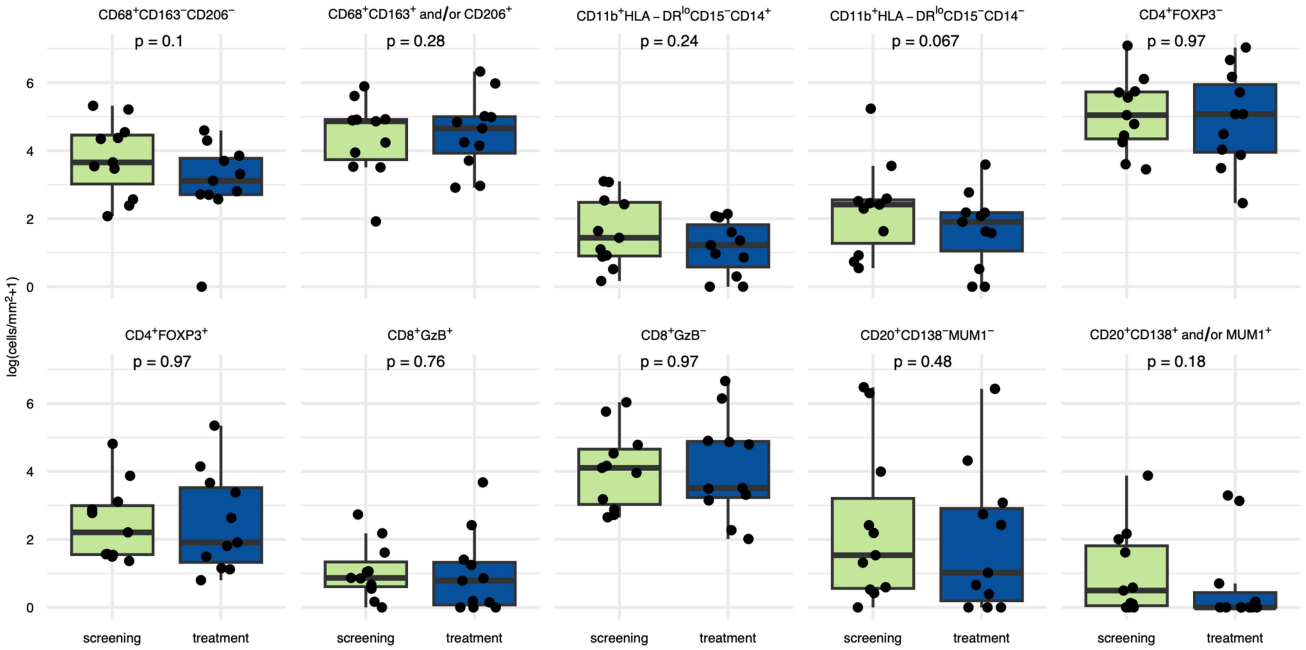

Extended Data Fig. 4 | Immune cell densities in CRPC biopsies with CXCR2 inhibition. Intratumor immune cells densities (log-transformed density (cells/mm^2)) in mCRPC biopsies taken during pre- (green) and on-treatment (blue), evaluating the immune cell subsets shown in all patients where on-target neutropenia (>30% mean decrease in neutrophils) was observed (n = 11 pairs). Data are represented by immune cell subset, individually, and as boxplots where the middle line is the median, the lower and upper hinges are the first and third quartiles, the upper whisker extends from the hinge to the largest value no further than 1.5 × interquartile range (IQR) from the hinge and the lower whisker extends from the hinge to the smallest value at most 1.5 × IQR from the hinge. Two-sided paired Wilcoxon signed-rank test p-values are shown.

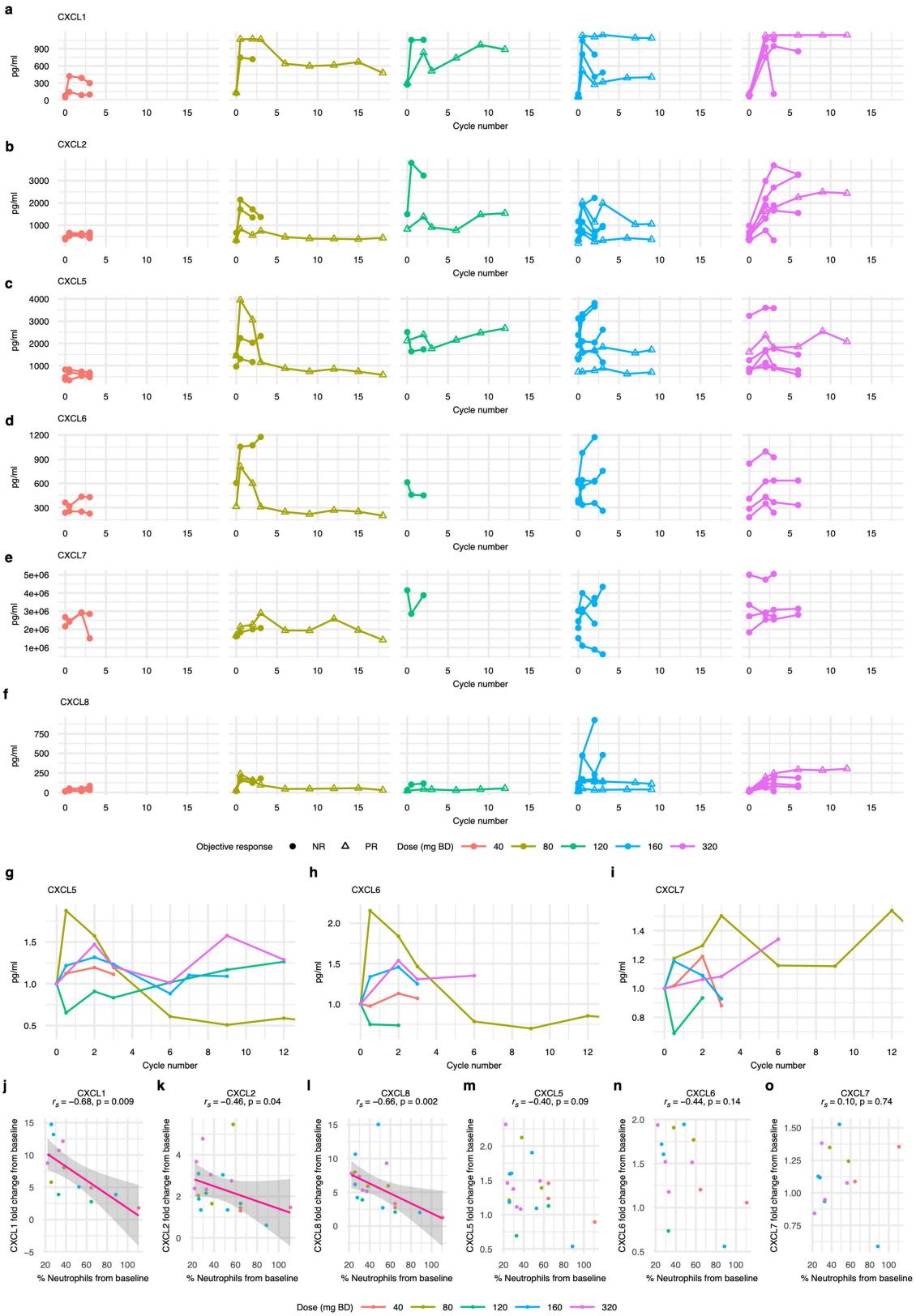

Extended Data Fig. 5 | See next page for caption.

Extended Data Fig. 5 | Blood CXCR1 and CXCR2 cytokines after CXCR2i and enzalutamide. a–**f**, Individual patient circulating levels of CXCL1 (n = 14), CXCL2 (n = 20), CXCL5 (n = 20), CXCL6 (n = 13), CXCL7 (n = 13), CXCL8 (n = 20) by dose level. Missing patients did not have samples collected or samples that failed quality control. **g**,**h**,**i**, By-dose level, mean fold change in circulating CXCL5 (**g**, n = 20), CXCL6 (**h**, n = 13), and CXCL7 (**i**, n = 13) levels compared with baseline over time. Samples were taken at baseline, on day 1 of each cycle and day 15 of the first cycle. **j**,**k**,**l**, Scatterplot of CXCL1 (**j**, n = 14), CXCL2 (**k**, n = 20), CXCL8 (**l**, n = 20) fold change from baseline versus percent blood neutrophil count from baseline on cycle 2 day 1. Estimated linear regression lines (pink) with 95% confidence interval (grey band), and correlation coefficients and p-values from the two-sided Spearman's rank correlation analyses are shown. **m**,**n**,**o**, Scatterplot of CXCL5 (n = 20) (**m**), CXCL6 (n = 13) (**n**), CXCL7 (n = 13) (**o**) fold change from baseline versus percent blood neutrophil count from baseline on cycle 2 day 1. Correlation coefficient and p-value from the two-sided Spearman's rank correlation test are shown. Colour of the lines and dots represent AZD5069 dose. NR = non-responder, PR = partial responder. BD = twice daily.

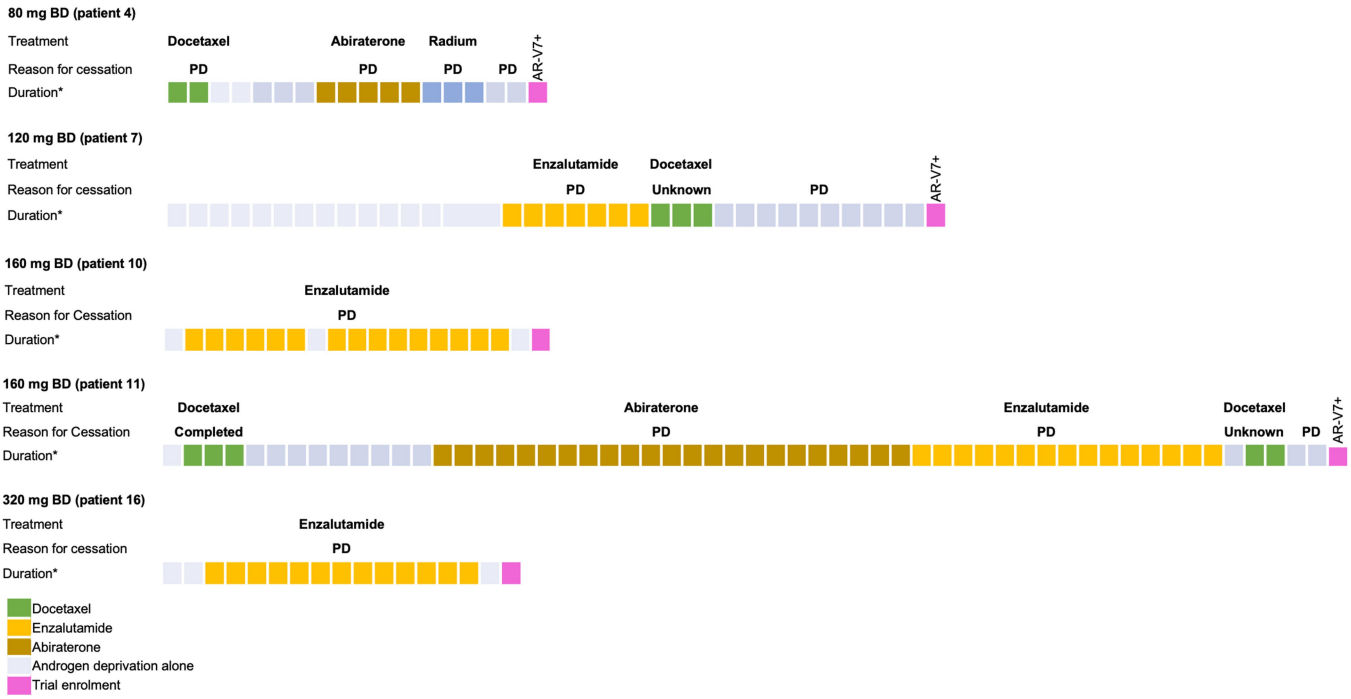

Extended Data Fig. 6 | Prior treatment history of responders. Systemic therapies administered after CRPC diagnosis in responders. Patients are ordered as per Fig. 4a. Each rectangle represents a two-month interval. All patients received androgen deprivation therapy throughout this period. Dose represents AZD5069 dose. AR-V7+ indicates the presence of AR-V7 protein expression in the pre-treatment CRPC biopsy. BD = twice daily.

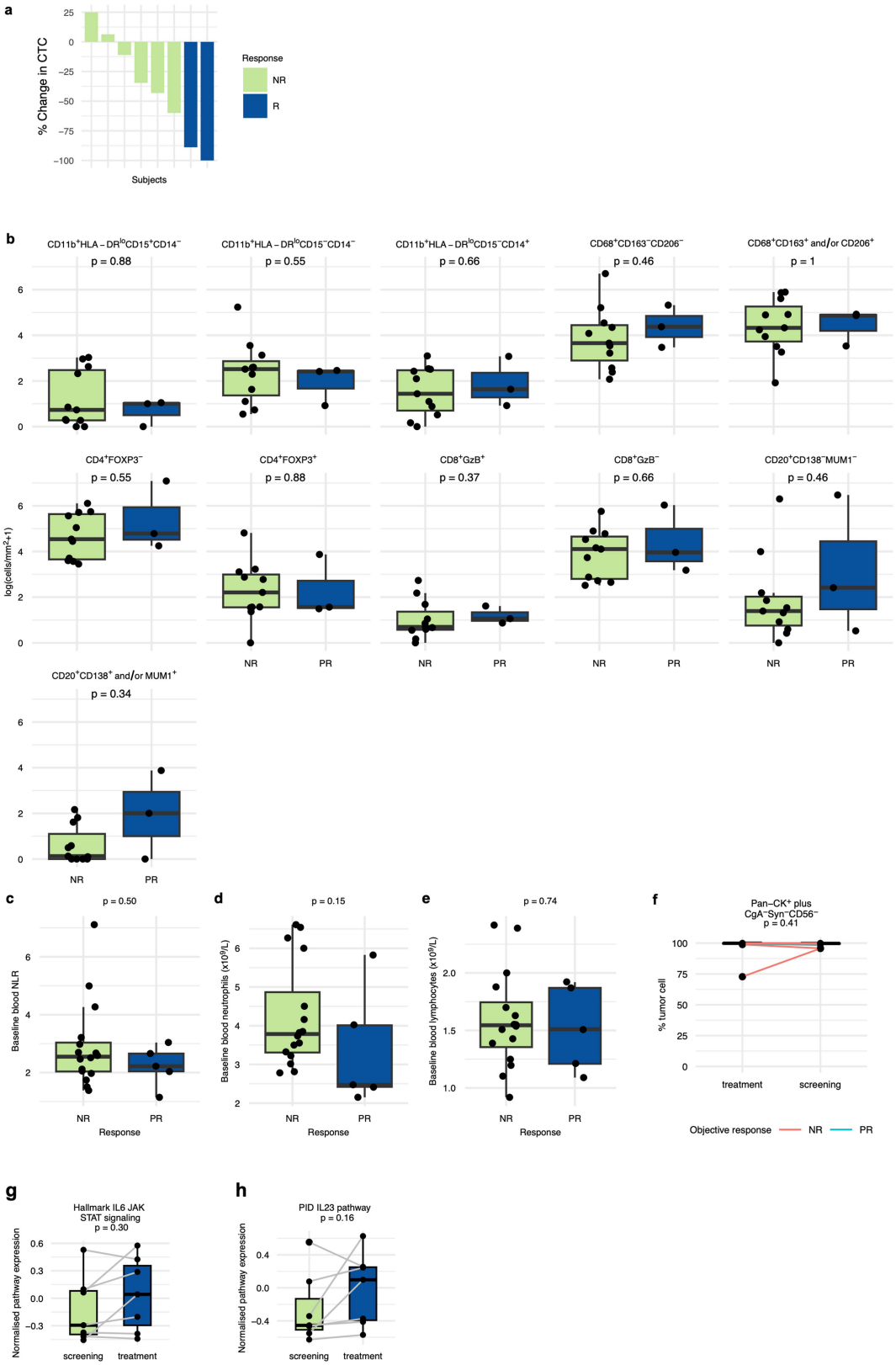

Extended Data Fig. 7 | See next page for caption.

Extended Data Fig. 7 | Biomarker and bulk RNAseq analyses. a, Waterfall plot showing maximum percentage CTC count decline from baseline in patients with CTC count ≥5 cells/7.5 ml at baseline. The two responding (R) patients with CTC count conversion from ≥5/7.5 ml of blood to <5 cells/7.5 ml of blood are shown in blue; patients also need to be on treatment for at least three cycles to be considered a responder. Non-responders (NR) are in green. **b**, Baseline immune cell densities (log-transformed (cells/mm^2)) in mCRPC biopsies of responders (n = 3) versus non-responders at baseline (n = 11). Missing patients did not have analysable paired tumour sample for analysis by IF assays. **c**,**d**,**e**, Baseline blood NLR (**c**), neutrophil (x10^9/L) (**d**), and lymphocyte (x10^9/L) (**e**) in responders (n = 5) versus non-responders (n = 16). In **b**–**e**, data are presented individually and as boxplots where the middle horizontal line is the median, the lower and upper hinges are the first and third quartiles, the upper whisker extend from the hinge to the largest value no further than 1.5 × interquartile range (IQR) from the hinge and the lower whisker extends from the hinge to the smallest value at most 1.5 × IQR from the hinge. Two-sided Mann-Whitney U test p-values are shown. **f**, Chromogranin (CgA)$^-$synaptophysin (Syn)$^-$CD56$^-$ pan-CK$^+$ cells as a proportion of all pan-CK$^+$ cells in paired tumour biopsies (n = 11 pairs). Lines link paired samples and colour denotes response. NR = non-responder (red), PR = partial responder (green). Two-sided paired Wilcoxon signed-rank test p-value is shown. **g**,**h**, Boxplot of gene expression of the Hallmark IL-6-JAK2-STAT3 signalling gene signature (**g**) and PID IL-23 signature (**h**) in RNA profiling data from paired CRPC biopsies with CD11b$^+$HLA-DR^{lo}CD15$^+$CD14$^-$ cell decrease (n = 7 pairs). In **g**,**h**, data are presented individually and with boxplots where the middle line is the median, the lower and upper hinges are the first and third quartiles, and the upper and lower whiskers extend from the hinge to the largest value no further than 1.5 × IQR from the hinge and the lower whisker extends from the hinge to the smallest value at most 1.5 × IQR from the hinge. Lines link paired, same-patient samples. Two-sided paired Wilcoxon signed-rank test p-values are shown.

Extended Data Table 1 | Baseline trial patient characteristics

Category	N=23[1]
Age (year): Median (Q1-Q3)	70.6 (66.2-73.2)
ECOG Performance Status, n (%)	
0	2 (8.7)
1	21 (91.3)
Gleason Score, n (%)	
< 8	6 (26.1)
8-10	13 (56.5)
Unknown	4 (17.4)
Primary tumour stage at diagnosis, n (%)	
T0	1 (4.3)
T1	1 (4.3)
T2	5 (21.7)
T3	9 (39.1)
T4	1 (4.3)
Unobtainable	6 (26.1)
Lymphadenopathy at diagnosis, n (%)	
N0	8 (34.8)
N1	7 (30.4)
Unobtainable	8 (34.8)
Metastasis at Diagnosis, n (%)	
Yes	12 (52.2)
No	9 (39.1)
Unobtainable	2 (8.7)
Prior radical therapies, n (%)	
Radiotherapy	5 (21.7)
Radical prostatectomy	1 (4.3)
Both	4 (17.4)
Unknown	13 (56.5)
Line of systemic therapy: Median (Q1, Q3)	4 (3-4)
Prior systemic therapy[2], n (%)	
Enzalutamide	20 (87.0)
Abiraterone	6 (26.1)
Apalutamide	1 (4.3)
Taxane	17 (73.9)
Cabazitaxel	7 (30.4%)
Radium 223	3 (13.0%)
Laboratory Results at Screening: Median (Q1-Q3)	
PSA (ng/ml)	219.5 (40.7-457.8)
Neutrophils (x 10^9/L)	3.54 (2.8-5.2)
NLR	2.7 (2.1-3.4)
Haemoglobin (x 10^9/L)	11.6 (10.8-11.9)
ALP (IU/L)	95 (85-169)

[1]Two patients were replaced and not evaluable for DLT because they ceased treatment likely due to disease progression, and not for a DLT before completing the DLT period.
[2]All patients received and progressed on ADT.
ECOG = Eastern Cooperative Oncology Group.

Extended Data Table 2 | Treatment-emergent adverse events

	40 mg BD (n=3)		80 mg BD (n=4)*		120 mg BD (n=3)		160 mg BD (n=6)		320 mg BD (n=7)*		All patients (n=23)	
TEAE, n (%)	All G	G≥3	All G	G≥3	All G	G≥3	All G	G≥3	All G	G≥3	All G	G≥3
Neutrophil decreased	2 (67)	0 (0)	3 (75)	1 (25)	3 (100)	2 (67)	5 (83)	4 (67)	6 (86)	4 (57)	19 (83)	11 (48)
Fatigue	0 (0)	0 (0)	1 (25)	0 (0)	1 (33)	0 (0)	2 (33)	0 (0)	3 (43)	0 (0)	7 (30)	0 (0)
Nausea	1 (33)	0 (0)	0 (0)	0 (0)	1 (33)	0 (0)	2 (33)	0 (0)	1 (14)	0 (0)	5 (22)	0 (0)
Anemia	1 (33)	0 (0)	0 (0)	0 (0)	1 (33)	0 (0)	2 (33)	1 (17)	0 (0)	0 (0)	4 (17)	1 (4)
Headache	0 (0)	0 (0)	0 (0)	0 (0)	0 (0)	0 (0)	0 (0)	0 (0)	3 (43)	0 (0)	3 (13)	0 (0)
White blood cell decreased	0 (0)	0 (0)	0 (0)	0 (0)	0 (0)	0 (0)	2 (33)	0 (0)	1 (14)	0 (0)	3 (13)	0 (0)
Constipation	0 (0)	0 (0)	0 (0)	0 (0)	1 (33)	0 (0)	0 (0)	0 (0)	1 (14)	0 (0)	2 (9)	0 (0)
Platelet decreased	0 (0)	0 (0)	0 (0)	0 (0)	1 (33)	0 (0)	1 (17)	0 (0)	0 (0)	0 (0)	2 (9)	0 (0)
Aphasia	0 (0)	0 (0)	0 (0)	0 (0)	0 (0)	0 (0)	0 (0)	0 (0)	1 (14)	0 (0)	1 (4)	0 (0)
Arthralgia	0 (0)	0 (0)	0 (0)	0 (0)	0 (0)	0 (0)	0 (0)	0 (0)	1 (14)	0 (0)	1 (4)	0 (0)
Aspartate aminotransferase increased	0 (0)	0 (0)	0 (0)	0 (0)	0 (0)	0 (0)	0 (0)	0 (0)	1 (14)	0 (0)	1 (4)	0 (0)
Death	0 (0)	0 (0)	0 (0)	0 (0)	0 (0)	0 (0)	0 (0)	0 (0)	1 (14)	1 (14)	1 (4)	1 (4)
Decreased appetite	0 (0)	0 (0)	0 (0)	0 (0)	0 (0)	0 (0)	0 (0)	0 (0)	1 (14)	0 (0)	1 (4)	0 (0)
Diarrhoea	0 (0)	0 (0)	0 (0)	0 (0)	0 (0)	0 (0)	0 (0)	0 (0)	1 (14)	1 (14)	1 (4)	1 (4)
Dry skin	0 (0)	0 (0)	0 (0)	0 (0)	0 (0)	0 (0)	0 (0)	0 (0)	1 (14)	0 (0)	1 (4)	0 (0)
Hypophosphataemia	0 (0)	0 (0)	1 (25)	0 (0)	0 (0)	0 (0)	0 (0)	0 (0)	0 (0)	0 (0)	1 (4)	0 (0)
Oedema genital	0 (0)	0 (0)	0 (0)	0 (0)	0 (0)	0 (0)	1 (17)	0 (0)	0 (0)	0 (0)	1 (4)	0 (0)
Pruritus	1 (33)	0 (0)	0 (0)	0 (0)	0 (0)	0 (0)	0 (0)	0 (0)	0 (0)	0 (0)	1 (4)	0 (0)
Skin infection	0 (0)	0 (0)	1 (25)	0 (0)	0 (0)	0 (0)	0 (0)	0 (0)	0 (0)	0 (0)	1 (4)	0 (0)
Vomiting	1 (33)	0 (0)	0 (0)	0 (0)	0 (0)	0 (0)	0 (0)	0 (0)	0 (0)	0 (0)	1 (4)	0 (0)

Treatment-emergent adverse events (TEAEs) were defined as adverse events that are definitely, highly likely, or possibly related to the investigational agents occurring at any time whilst a patient was on study.

Data are n (%). Treatment-related adverse events of 23 patients were included the safety analysis.

G = grade according to NCI CTCAE v4.0.

*Two of 23 patients were not evaluable for DLT due to early cessation of the study drugs due to progressive disease before completing the DLT period; one patient died on study likely due to progressive disease after 6 days on study.

nature portfolio

Corresponding author(s): Johann de Bono

Last updated by author(s): 08/31/2023

Reporting Summary

Nature Portfolio wishes to improve the reproducibility of the work that we publish. This form provides structure for consistency and transparency in reporting. For further information on Nature Portfolio policies, see our Editorial Policies and the Editorial Policy Checklist.

Statistics

For all statistical analyses, confirm that the following items are present in the figure legend, table legend, main text, or Methods section.

n/a	Confirmed	
☐	☒	The exact sample size (*n*) for each experimental group/condition, given as a discrete number and unit of measurement
☒	☐	A statement on whether measurements were taken from distinct samples or whether the same sample was measured repeatedly
☐	☒	The statistical test(s) used AND whether they are one- or two-sided *Only common tests should be described solely by name; describe more complex techniques in the Methods section.*
☐	☒	A description of all covariates tested
☐	☒	A description of any assumptions or corrections, such as tests of normality and adjustment for multiple comparisons
☐	☒	A full description of the statistical parameters including central tendency (e.g. means) or other basic estimates (e.g. regression coefficient) AND variation (e.g. standard deviation) or associated estimates of uncertainty (e.g. confidence intervals)
☐	☒	For null hypothesis testing, the test statistic (e.g. *F*, *t*, *r*) with confidence intervals, effect sizes, degrees of freedom and *P* value noted *Give P values as exact values whenever suitable.*
☒	☐	For Bayesian analysis, information on the choice of priors and Markov chain Monte Carlo settings
☒	☐	For hierarchical and complex designs, identification of the appropriate level for tests and full reporting of outcomes
☐	☒	Estimates of effect sizes (e.g. Cohen's *d*, Pearson's *r*), indicating how they were calculated

Our web collection on statistics for biologists contains articles on many of the points above.

Software and code

Policy information about availability of computer code

Data collection

Clinical trials data was collected in MACRO (v4.11.0.459).
SAE data was recorded in Safire (v3.0).
Translational singleplex immunohistochemical was collected using Progeny (v10).
CTC count data was collected in Microsoft Excel (v16.75).
PK and ELISA data were collected and stored using Microsoft Excel (v16.73).
Circulating cytokine data was collected using Luminex xPONENT (v3.1) and EnVision (v1.14.3049.528) and then output into Microsoft Excel v16.75).
Multiplex IF data was collected in Halo (v3.6.4134.137)
Hyperplex IF data was collected in the COMET Control Software (v 0.70.0.1) then imported and stored in Halo (v3.6.4134.137).

Data analysis

Statistical analysis for the clinical trial was performed using R software (v4.2.2) and according to the Statistical Analyses Plan for trial-related analyses.

Somatic variant calls from the Next-generation sequencing data were manually inspected in the Integrative Genomics Viewer (v2.16.1).

HTG data were analysed using the HTG EdgeSeq Parser Software (V5.3, HTG Molecular Diagnostics). Differential gene expression between pre and post treatment samples was performed using the HTG EdgeSeq Reveal DESeq2 analysis pipeline and R Software (v4.2.3).

The SU2C/PCF transcriptomes were aligned to the human reference genome (GRCh37/hg19) using TopHat2 (v2.0.7). Gene expression as

fragments per kilobase of transcript per million mapped reads (FPKM) was calculated using Cufflinks (v2.2.1).

For the single-cell transcriptomic data analyses, publicly available data was analysed in R Software (v4.1.3). The raw counts from the localized prostate cancer data were log normalized. Both datasets were processed with Seurat (v4.3.0) and underwent scaling, clustering, dimensional reduction, and cell type assignment with SingleR (v1.8.1) using the Blueprint ENCODE reference dataset from the celldex (v1.4.0) library.

Pharmacokinetic parameters were calculated using non-compartmental analysis (Phoenix v8.1, Certara).
IF data were analysed in Halo v3.6.4134.137) and R software (v4.2.2).
All correlative translational analyses and survival analyses were performed using R software (v4.2.2).
Correlative analyses of PK-PD-dose relationships were performed using R software (v4.2.2).

For manuscripts utilizing custom algorithms or software that are central to the research but not yet described in published literature, software must be made available to editors and reviewers. We strongly encourage code deposition in a community repository (e.g. GitHub). See the Nature Portfolio guidelines for submitting code & software for further information.

Data

Policy information about availability of data

All manuscripts must include a data availability statement. This statement should provide the following information, where applicable:

- Accession codes, unique identifiers, or web links for publicly available datasets
- A description of any restrictions on data availability
- For clinical datasets or third party data, please ensure that the statement adheres to our policy

Source data for the non-clinical trial related translational analyses are provided in the source data file associated with each figure (except for when the data was downloaded from the publicly available datasets listed below). The full study protocol is provided with this paper as part of the supplementary information.

Bulk RNASeq data from the SU2C/PCF cohort (https://www.pnas.org/doi/10.1073/pnas.1902651116) was downloaded from https://www.cbioportal.org/study/summary?id=prad_su2c_2019. Single-cell transcriptomic data from 15 mCRPC samples (https://www.nature.com/articles/s41591-021-01244-634) were downloaded from https://singlecell.broadinstitute.org/single_cell/study/SCP1244/transcriptional-mediators-of-treatment-resistance-in-lethal-prostate-cancer (study number SCP1244).

Single-cell transcriptomic data from 11 patients with localized prostate cancer (https://www.nature.com/articles/s41467-021-27322-435) were downloaded from https://www.ncbi.nlm.nih.gov/geo/query/acc.cgi?acc=GSE176031 (GEO accession GSE176031).

De-identified, bulk RNASeq data from the RMH cohort may be requested from the corresponding author (J.S.dB.). Request for data must provide clinically relevant rationale and will be reviewed by the corresponding author (J.S.dB.) to determine if the request is subject to any ethical and/or confidentiality considerations. Subject to patient privacy and confidentiality obligations, access to data from the clinical trial may be available upon request to the study sponsor (The ICR, ACE@icr.ac.uk) and corresponding author (J.S.dB). Request data must provide clinically relevant rationale in adherence with the intent of the study and patients' consent, will be reviewed by the study sponsor and the corresponding author (J.S.dB.) to determine if the request is subject to any intellectual property, ethical and/or confidentiality considerations, and will respond promptly. Patient identifiers or information that may reveal the patient's identity will not be shared owing to patient confidentiality. Any data or material that can be shared will be done via a material transfer agreement with The ICR.

Research involving human participants, their data, or biological material

Policy information about studies with human participants or human data. See also policy information about sex, gender (identity/presentation), and sexual orientation and race, ethnicity and racism.

Reporting on sex and gender	Since our study only included patients with histologically proven prostate cancer, all participants were of male sex. Gender data was not collected from any of the participants.
Reporting on race, ethnicity, or other socially relevant groupings	No socially constructed or socially relevant categorization variables were collected or used.
Population characteristics	For the clinical trial, 23 participants with histologically confirmed metastatic castration-resistant prostate cancer were enrolled. Participants were recruited from the following participating study sites: The Royal Marsden Hospital (UK), Oncology Institute of Southern Switzerland (Switzerland), and Belfast City Hospital Cancer Centre (Northern Ireland). Description of this cohort is presented in Extended Data Table 1. For the translational analyses of myeloid cell infiltration, we studied two cohorts of patients with metastatic prostate cancer were included. The first cohort (cohort 1) consisted of 48 mCRPC biopsies from patients treated at The ICR/RMH, IOSI, and Belfast City Hospital. The validation cohort consisted of another 57 mCRPC biopsies from patients treated at the RMH. Descriptions of these 2 cohorts are presented in Supplementary Table S1.
Recruitment	Participants were recruited from 3 oncology centres in Europe (The Royal Marsden Hospital, Belfast City Hospital, and Oncology Institute of Southern Switzerland). Patients with metastatic prostate cancer were either referred to the study site for consideration of participation in an oncology clinical trials by their oncologist or the patients were already under the care their treating oncologist located at the study site. The study investigator determined, in consultation with the patient, whether they wished to participate in an early phase clinical trial, and if there was no clear contraindication to participating in the trial, and the patient was interested in considering this option, the patient was provided with written and verbal information about the study. This information includes, but was not limited to: information about the study drugs and treatment schedule; the scientific and clinical rationale for the study; potential risks and benefits; assessments and schedule during screening, on trial, and after trial drug cessation; and how data and samples were to be stored, used, and disseminated. Patients were aware that participation in the study is entirely voluntary and that they could withdraw their consent at any point. Patients were made aware of potential alternatives to participating in the study, including opting for no

	further active intervention. Patients were given subsequent opportunities for additional questions to be addressed with the study physician and ample time to make the decision. Potential biases: only patients who were treated at or referred to one of the study sites, which were all cancer centres in Europe that conducted early phase trials, were included. All participants had to meet the specific inclusion/exclusion criteria of the trial which excluded patients with worse performance status, major organ dysfunction, history of other malignancies, and comorbidities (see details in the Methods section). A part of the study was conducted during the Covid-19 pandemic, which may impact some patients' willingness to participate in clinical trials. All of these factors may have impacted the generalizability of these findings to the broader, global, advanced prostate cancer population, and therefore the findings of our study warrant further evaluation in other contexts, and with larger and more diverse cohorts.
Ethics oversight	Clinical trial oversight: The study was conducted in accordance with the provisions of the Declaration of Helsinki and Good Clinical Practice guidelines. Regulatory approvals were obtained from the Medicines Healthcare products Regulatory Agency (MHRA), Swiss Swissmedic, and local Research Ethics Committees (London-Surrey Borders REC for the Royal Marsden Hospital and Belfast City Hospital; Comitato Etico Cantonale Bellinzona for the Oncology Institute of Southern Switzerland in Switzerland). Written informed consent was obtained from all participants. No participant compensation was provided. A safety review committee evaluated the safety and tolerability at regular intervals after recruitment of three patients to a schedule. All protocol amendments were approved by the trial sponsor, MHRA, Swissmedic, and UK and Swiss RECs (London-Surrey Borders REC for the Royal Marsden Hospital and Belfast City Hospital; Comitato Etico Cantonale Bellinzona for the Oncology Institute of Southern Switzerland in Switzerland). The study was sponsored and monitored by The Institute of Cancer Research (The ICR), UK. The study was registered on ClinicalTrials.gov before commencement (ClinicalTrials.gov identifier: NCT03177187, EudraCT: 2016-003141-28). All patients included in the translational analyses provided informed consent, and enrolled onto institutional protocols approved by the local RECs at The Royal Marsden Hospital, Belfast City Hospital, and Institute of Oncology of Southern Switzerland.

Note that full information on the approval of the study protocol must also be provided in the manuscript.

Field-specific reporting

Please select the one below that is the best fit for your research. If you are not sure, read the appropriate sections before making your selection.

☒ Life sciences ☐ Behavioural & social sciences ☐ Ecological, evolutionary & environmental sciences

For a reference copy of the document with all sections, see nature.com/documents/nr-reporting-summary-flat.pdf

Life sciences study design

All studies must disclose on these points even when the disclosure is negative.

Sample size	For the phase 1 trial, sample size was chosen pragmatically. According to the rule-based 3+3 design, which guided dose-escalation decisions, the cohort size was three patients and skipping of dose levels in dose-escalation was not allowed. For the translational studies, sample size was also determined pragmatically based on available prostate cancer biopsy cohorts as well as the size of the existing RNASeq datasets.
Data exclusions	No data was excluded. Analyses were performed as per study protocol. The evaluable populations were defined as per protocol.
Replication	For the translational analyses pertaining to associations between NLR and neutrophils and myeloid cell count as well as NLR and neutrophils and myeloid gene signatures, and survival analyses, a second independent cohort was analysed to validate the initial findings.
Randomization	The study utilised the 3+3 design where participants were enrolled sequentially to escalating dose levels, and does not allow for randomisation.
Blinding	Blinding from patients: It would not have been clinically acceptable to the patient or their physician to administer placebos (inactive treatments) in the context of a phase 1 oncology clinical trial where the trial is logistically intensive, carry uncertainties, and the patients have limited life expectancies, and therapeutic options, therefore all patients were assigned to receive the active study drug. Patients were not blinded to the dose-level they were receiving. Given this is a phase 1 study testing a drug combination that has not previously been assessed, we also wanted to be transparent with patients about the dose level they were to receive, and the emerging clinical experience, as this could factor into patients' risk-benefit considerations for whether to participate in an early phase clinical trial. Blinding from investigators: It would not be feasible or safe to blind the dose level from the investigators in a 3+3 design phase 1 trial given investigators participate in safety review meetings where dose-escalation decisions are made and patients are enrolled sequentially to escalating dose levels.

Reporting for specific materials, systems and methods

We require information from authors about some types of materials, experimental systems and methods used in many studies. Here, indicate whether each material, system or method listed is relevant to your study. If you are not sure if a list item applies to your research, read the appropriate section before selecting a response.

Materials & experimental systems

n/a	Involved in the study
☐	☒ Antibodies
☐	☒ Eukaryotic cell lines
☒	☐ Palaeontology and archaeology
☒	☐ Animals and other organisms
☐	☒ Clinical data
☒	☐ Dual use research of concern
☒	☐ Plants

Methods

n/a	Involved in the study
☒	☐ ChIP-seq
☒	☐ Flow cytometry
☒	☐ MRI-based neuroimaging

Antibodies

Antibodies used

HYPERPLEX IF
--- Primary antibodies (see Supplementary information for further details)
Listed in order of marker, vendor, cat number, clone, lot number
NCAM1 (CD56), Abcam, ab270248, 123C3.D5, 1020624-1
CXCR2, Abcam, ab245982, EPR22301-103, GR3378654-6
FOXP3, eBioscience™ (Thermo Fisher), 14-4777-82, 236A/E7, 2378013
CD15, Dako, M3631, Carb-3, 11397463
Granzyme B, CST, 46890, D6E9W, 6
CD14, Abcam, ab133503, EPR3652, GR211954-7
CD138, Dako, M7228, MI15, 41415171
CD11b, Abcam, ab52478, EP1345Y, GR3219233-5
MUM1, Dako, M7259, MUM1p, 41455977
CD8, Dako, M7103, C8/144B, 41389238
CD163, Abcam, ab182422, EPR19518, GR3339055-17
CD68, Dako, M0876, PG-M1, 41337737
Chromogranin A, Dako, M0869, DAK-A3, 41449632
HLA-DR, Abcam, ab20181, TAL 1B5, GR3378141-4
CD4, Abcam, ab133616, EPR6855, GR3276764-30
Pan-cytokeratin, Dako, M3515, AE1/AE3, 11445606
CD20, Dako, M0755, L26, 41367309
CD38, Abcam, ab226034, EPR4106, GR3402044-1
Synaptophysin, Leica Biosystems, SYNAP-299-L-CE, 27G12, 6081141
CD206/MRC1, CST, 91992, E2L9N, 1
--- Secondary antibodies
Listed in order of marker, vendor, cat number, clone, lot number
Goat anti-Mouse IgG (H+L) Highly Cross-Adsorbed Secondary Antibody, Alexa Fluor™ Plus 555, Invitrogen (Thermo Fisher Scientific), A32727, Polyclonal, WL333735
Goat anti-Rabbit IgG (H+L) Highly Cross-Adsorbed Secondary Antibody, Alexa Fluor™ Plus 647, Invitrogen (Thermo Fisher Scientific), A32733, Polyclonal, WL333739

MULTICOLOR IF
--- Primary antibodies
Listed in order of marker, vendor, cat number, clone, lot number
CXCR2, Abcam, ab245982, EPR22301-103, GR3378654-5
CD11b, Abcam, ab52478, EP1345Y, GR3219233-10
CD15, Dako, M3631, Carb-3, 11397463
CD14, Abcam, ab133503, EPR3652, GR211954-8
HLA-DR, Abcam, ab20181, TAL.1B5, GR3456090-1

-- Detection System:
Novocastra Post Primary, Leica Biosystems, Novolink Max Polymer Detection System, RE7280-K, 6098453
Novolink Polymer, Leica Biosystems, Novolink Max Polymer Detection System, RE7280-K, 6098453
TSA Coumarin, Akoya Biosciences, 1:50, NEL703001KT, 20220408
OPAL 520, Akoya Biosciences, 1:300, NEL820001KT, 20212719
OPAL 570 Akoya Biosciences, 1:300, NEL820001KT, 20213431
OPAL 650, Akoya Biosciences, 1:300, FP1496001KT, 20211913
TSA-DIG, Akoya Biosciences, 1:200, FP1501001KT, 20212315
OPAL 780, Akoya Biosciences, 1:50, FP1501001KT, 20213604

SINGLEPLEX IHC
Listed in order of marker, vendor, cat number, clone, lot number
PTEN, CST, Rabbit, 9559, 138G6, 17 and lot 19
AR-V7, Revmab, Rabbit, 31-1109-00, RM7, S-08-02447 and V-06-05221

Validation

https://www.abcam.com/products/primary-antibodies/ncam1-antibody-123c3d5-ab270248.html
https://www.abcam.com/products/primary-antibodies/cxcr2-antibody-epr22301-103-bsa-and-azide-free-ab245982.html
https://www.thermofisher.com/antibody/product/FOXP3-Antibody-clone-236A-E7-Monoclonal/14-4777-82
https://www.agilent.com/en/product/immunohistochemistry/antibodies-controls/primary-antibodies/cd15-%28concentrate%

29-76600
https://www.cellsignal.com/products/primary-antibodies/granzyme-b-d6e9w-rabbit-mab/46890
https://www.abcam.com/products/primary-antibodies/cd14-antibody-epr3652-ab133503.html
https://www.agilent.com/en/product/immunohistochemistry/antibodies-controls/primary-antibodies/cd138-%28concentrate%29-76642
https://www.abcam.com/products/primary-antibodies/cd11b-antibody-ep1345y-c-terminal-ab52478.html
https://www.agilent.com/en/product/immunohistochemistry/antibodies-controls/primary-antibodies/mum1-protein-%28concentrate%29-76652
https://www.agilent.com/en/product/immunohistochemistry/antibodies-controls/primary-antibodies/cd8-%28concentrate%29-76631
https://www.abcam.com/products/primary-antibodies/cd163-antibody-epr19518-ab182422.html
https://www.agilent.com/en/product/immunohistochemistry/antibodies-controls/primary-antibodies/cd68-%28concentrate%29-76550
https://www.agilent.com/en/product/immunohistochemistry/antibodies-controls/primary-antibodies/chromogranin-a-%28concentrate%29-76546
https://www.abcam.com/products/primary-antibodies/hla-dr-antibody-tal-1b5-ab20181.html
https://www.abcam.com/products/primary-antibodies/cd4-antibody-epr6855-ab133616.html
https://www.agilent.com/en/product/immunohistochemistry/antibodies-controls/primary-antibodies/cytokeratin-%28concentrate%29-76562
https://www.agilent.com/en/product/immunohistochemistry/antibodies-controls/primary-antibodies/cd20cy-%28concentrate%29-76520
https://www.abcam.com/products/primary-antibodies/cd38-antibody-epr4106-bsa-and-azide-free-ab226034.html
https://shop.leicabiosystems.com/en-gb/ihc-ish/ihc-primary-antibodies/pid-synaptophysin
https://www.cellsignal.com/products/primary-antibodies/cd206-mrc1-e2l9n-rabbit-mab/91992

https://www.cellsignal.com/products/primary-antibodies/pten-138g6-rabbit-mab/9559?_requestid=2919710
https://www.revmab.com/index.php/product/anti-androgen-receptor-ar-v7-specific-rabbit-monoclonal-antibody-clone-rm7-arv7-splice-variant/?gclid=EAIaIQobChMIhK_L98TzgAMVkM7CBB13HQf1EAAYASAAEgK8bfD_BwE

Antibodies against CXCR2, FOXP3, CD15, CD14, CD138, CD11b, MUM1, CD163, CD68, HLA-DR, CD4, CD38, CD206, CD8, and granzyme-B were validated by Western blot comparing detection of protein expression in whole cell lysates treated with either nontargeting control siRNA or ON-TARGETplus pooled siRNA against the target protein (Dharmacon) or using positive and negative control cell lines. All markers were validated for appropriate tissue localisation on immunohistochemical staining of relevant positive and negative tissue controls and reviewed by a certified pathologist (B.G.). Validation for PTEN, CD4, CD8, FOXP3, CD11b, CD15, CD138, CD20, synaptophysin, chromogranin and AR-V7 were as previously described. IHC was performed on FFPE tissue sections using an automated staining platform (Bond RX, Leica Biosystems). Bone biopsies were decalcified using pH 7 EDTA for 48 hours at 37oC. Once validated for target sensitivity and specificity, the antibodies were further optimised for IHC, multi-/hyperplex IF using methods described below. The full list of antibodies, working dilutions, and incubation times are in Supplementary Tables S7 and S8.

Eukaryotic cell lines

Policy information about cell lines and Sex and Gender in Research

Cell line source(s)	All cell lines were purchased from ATCC (https://www.atcc.org). Cell lines used for antibody validation include: LNCaP, HL-60, HeLa, Daudi, Thp1, Jurkat, HDML2, A-431, A549, TIME
Authentication	Cell lines were authenticated by STR profiling prior to use
Mycoplasma contamination	All cells were regularly tested for mycoplasma contamination and were negative (every 3 months).
Commonly misidentified lines (See ICLAC register)	No commonly misidentified cell lines were use.

Clinical data

Policy information about clinical studies

All manuscripts should comply with the ICMJE guidelines for publication of clinical research and a completed CONSORT checklist must be included with all submissions.

Clinical trial registration	NCT03177187
Study protocol	Submitted with the manuscript
Data collection	The trial was conducted at three centres in Europe (Royal Marsden Hospital (UK), Belfast City Hospital (UK), The Oncology Institute of Southern Switzerland (Switzerland). The trial was conducted between November 2017 and November 2022.
Outcomes	Primary endpoint: 1. To identify the dose-limiting toxicities (DLTs), estimate the maximum tolerated dose (MTD) and identify the recommended phase II dose (RP2D) or the recommended phase II doses (RP2Ds) of AZD5069 administered in combination with enzalutamide at 160mg OD. -Adverse event (toxicity) evaluation (history and examination) was performed by the study investigator (medical oncologist) on a weekly basis, and more frequently if required, during the DLT period (cycle 1) as well as during cycle 2 of the study, and then at least once every 4 weeks thereafter. -Adverse events were graded using the National Cancer Institute (NCI) CTCAE (v4.0) criteria. -The DLT and MTD were adverse events defined using the NCI CTCAE v4.0 criteria (full list of definitions are listed in the protocol,

section 3.2) that were deemed highly probably or probably related to either study drug by the study investigator.

Secondary endpoints:
1. Antitumor activity was defined by the rate of objective response. If any of these occur, patients will be considered to have responded:
---- PSA decline ≥ 50% criteria confirmed 4 weeks or later and/or,
---- confirmed soft tissue objective response by RECIST (v1.1) in patients with measurable disease and/or,
---- ONLY for patients with detectable circulating tumour cell count (CTC) of ≥5/7.5ml blood at baseline, conversion of CTC <5/7.5ml blood nadir.
----Patients must receive 12 weeks of trial treatment to be considered to have responded. .
--Disease progression is defined as:
----Progression of soft tissue/visceral disease by RECIST (v1.1) and/or,
----Progression of bone disease by PCWG2 bone scan criteria and/or,
----Progression of PSA by PCWG2 PSA criteria and/or
----Unequivocal clinical progression.
2 rPFS was be measured from the date of AZD5069 addition to enzalutamide until:
-- Progression of soft tissue/visceral disease by RESIST and/or,
-- progression of bone disease by PCWG2 bone scan criteria and/or,
-- death from any cause
3. OS was be measured from the date of AZD5069 addition to enzalutamide to the date of death (whatever cause).
4. Determination of the plasma levels of enzalutamide and AZD5069 using validated assays
5. Identify those patients with a NLR ≥ 3 (at baseline) that convert to an NLR < 3 (blood nadir) with AZD5069 and enzalutamide in combination.
6. Identify those patients whose circulating myeloid derived suppressor cells (MDSCs) and intratumoral MDSCs reduce by 50%

Key exploratory endpoints:
1. Evaluating the effect of AZD5069 treatment on circulating cytokine levels in whole blood using an enzyme-linked immunosorbent assay (ELISA).
2. Evaluation of the impact of CXCR2i depending on tumor molecular profile, such as PTEN loss.

Radiologic tumor responses were measured by CT of the thorax, abdomen, and pelvis bone scan and bone scan, and where indicated, whole body magnetic resonance imaging, at baseline, once every 3 cycles, then at the end of treatment if this was more than eight weeks since the last scan. PSA and CTC count were measured at baseline, then on day 1 of every cycle and at the end of treatment visit. PSA responses were determined by PCWG2 criteria. CTC counts were analysed using previously described methods (Mateo et al., NEJM, 2015, Goodall et al., Cancer Discovery, 2017). Patients need to be on trial for at least 12 weeks to be considered to have responded. NLR was a quotient of the neutrophil and lymphocyte count taken on study (from routine hematology bloods at baseline and serially on day 1 of every cycle). Immune cell densities were determined by IF of pre and on-treatment biopsies taken before and after starting trial treatment. All slides were QC'd and reviewed by the pathologist (BG) and histopathology scientist (MC). PK data were obtained from PK bloods taken at prespecified time points (baseline, start of cycle 1 and 2) evaluating for plasma levels of enzalutamide and AZD5069 for patients in dose levels 1-4 . Bloods for serum cytokine analyses were collected at prespecified timepoints per the trial protocol (baseline, day 1 of every cycle, and day 15 of the first cycle).